J. Fluid Mech. (2014), *vol.* 748, *pp.* 549–579. © Cambridge University Press 2014
doi:10.1017/jfm.2014.191

Vortex shedding and heat transfer in rotationally oscillating cylinders

Prabu Sellappan† and Tait Pottebaum

Department of Aerospace and Mechanical Engineering, University of Southern California, Los Angeles, CA 90089, USA

(Received 28 October 2013; revised 27 March 2014; accepted 2 April 2014; first published online 1 May 2014)

Wake formation and heat transfer from a rotationally oscillating circular cylinder in cross-flow at $Re = 750$ are studied. Two aspects, the effect of cylinder forcing on vortex shedding and the effect of the wake structures on convective heat transfer, are studied. Cylinder forcing conditions range between $0.09 \leqslant \theta_{PP} \leqslant 2.09$, where θ_{PP} is the peak-to-peak oscillation amplitude in radians and $0.70 \leqslant F_R \leqslant 3.16$, where F_R is the ratio of forcing frequency to natural shedding frequency. Digital particle image velocimetry (DPIV) is used to obtain quantitative wake structure information. Wake modes, and regions of the parameter space in which they occur, are identified for both heated and unheated cylinders. For the heated cylinder, cylinder forcing is found to affect the convective heat-transfer rate. Certain wake modes, including newly discovered wake modes synchronized over multiple oscillation cycles, are found to correlate with significant heat-transfer enhancement. Cylinder tangential velocity is also found to affect the heat-transfer rate in certain regions of the parameter space.

Key words: convection, vortex shedding, wakes/jets

1. Introduction

Vortex shedding from bluff bodies is observed frequently in nature and in many practical engineering applications. It has been observed in flows around tall buildings, submarine periscopes and large-scale flows such as those around mountain peaks. The alternate shedding of vortices leads to structural vibrations, which can lead to resonance and failure of the structure in some cases (Williamson 1996). Such vortex-induced vibration is also known to occur in industrially important devices such as tube-bank heat exchangers. In such cases, there is a strong coupling between the vortex shedding and heat transfer, accompanied by significant heat-transfer enhancement under certain forcing conditions and it is important to understand the relationship between them in order to improve the safety and efficiency of heat exchangers. This requires an understanding of the mechanism by which vortex shedding occurs and methods to control the vortex shedding. One method that has proven to be effective as a control strategy for smooth cylinders placed in cross-flow is cylinder forcing. Rotary oscillations, as compared with transverse or streamwise oscillations, are especially advantageous in the case of applications with severe space constraints. Despite its importance, the effect of rotary oscillations on vortex

† Email address for correspondence: psellapp@usc.edu

https://doi.org/10.1017/jfm.2014.191 Published online by Cambridge University Press

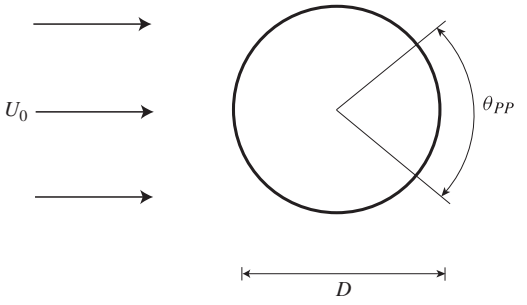


FIGURE 1. Schematic of basic set-up.

shedding is still not fully understood and very little is known regarding the actual wake structure or heat transfer under such forcing conditions.

This study looks at rotationally oscillating cylinders placed in a cross-flow. A schematic of the basic set-up is shown in figure 1. An important non-dimensional parameter is the Reynolds number, defined as $Re = U_0 \cdot D/\nu$, where U_0 is the free-stream velocity, D is the cylinder diameter and ν is the kinematic viscosity of the fluid. Another important parameter is the non-dimensional shedding frequency, or Strouhal number, $St = f_S \cdot D/U_0$, where f_S is the natural shedding frequency or Strouhal frequency of the unforced cylinder at a given Re. The cylinder forcing can be described in terms of the non-dimensional frequency ratio, $F_R = f_f/f_S$, where f_f is the forcing frequency and θ_{PP} is the peak-to-peak oscillation amplitude in radians.

1.1. *Vortex shedding from cylinders*

Vortex shedding from stationary, smooth, circular cylinders has been studied extensively due to their simple, well-defined geometric shape. The wake formed due to flow past a circular cylinder is considered as a baseline case for more complex flows and geometries. One early paper that looked at high-Reynolds-number flows is by Roshko (1961). This experimental study performed in a pressurized wind tunnel looked at flows around a stationary cylinder for $Re = 10^6$–10^7. Szepessy & Bearman (1992) looked at aspect ratio effects on the vortex shedding from smooth, circular cylinders at high Reynolds numbers ($Re = 8000$–$140\,000$). Recently, Norberg (2001) studied flows around a stationary cylinder for $Re = 47$–$220\,000$ and gave an empirical correlation between the Reynolds number and Strouhal number. Empirical relationships between St and Re over limited ranges of Re have also been proposed by Bearman (1969), Williamson (1988), Eisenlohr & Eckelmann (1989), Hammache & Gharib (1989), Norberg (1994), Kwon & Choi (1996) and Posdziech & Grundmann (2007). An explanation for this relationship between Re and St, based on the concept of a universal Strouhal number, was provided by Roshko (1954, 1955). A comprehensive review of stationary cylinder wakes can be found in Williamson (1996).

Many studies over the last two decades have focused on vortex shedding from cylinders undergoing forced oscillations in various configurations. Nishihara, Kaneko & Watanabe (2005) studied cylinders undergoing streamwise oscillations at $Re = 17\,000$ and $Re = 34\,000$. Williamson & Roshko (1988) studied cylinders undergoing transverse oscillations at $300 \leqslant Re \leqslant 1000$ and identified the vortex shedding patterns, shown in figure 2, in terms of the number and relative arrangement of vortices shed over one oscillation cycle. A vortex pair, consisting of two

https://doi.org/10.1017/jfm.2014.191 Published online by Cambridge University Press

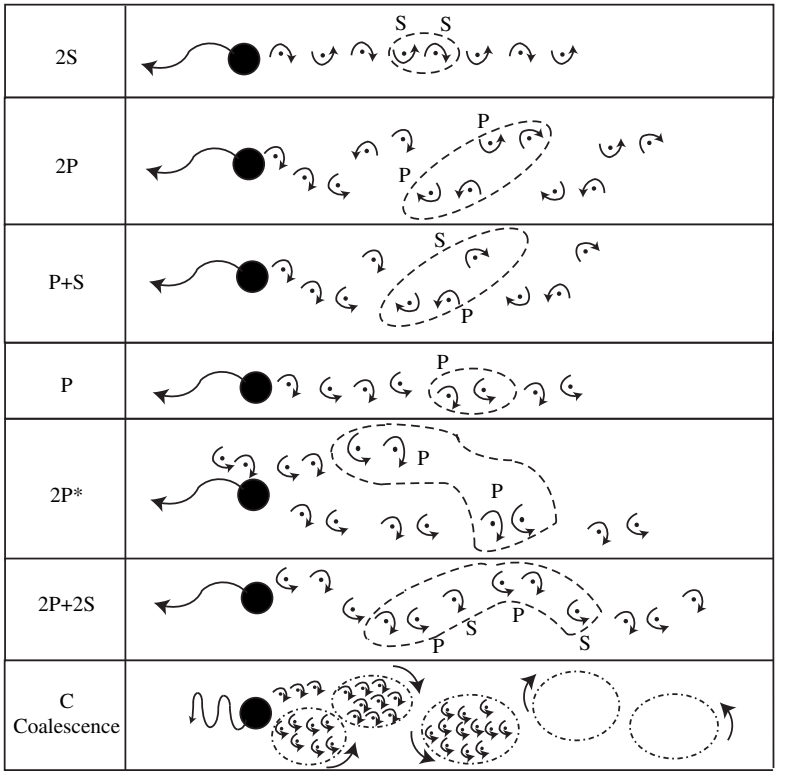


FIGURE 2. Sketches of the vortex shedding patterns from Williamson & Roshko (1988). The dashed curve encircles the vortices shed in one complete cycle. P denotes a vortex pair and S denotes a single vortex. Redrawn to improve print quality and is qualitatively similar to the original figure.

counter-rotating vortices is defined as 'P', a single vortex is defined as 'S' and the various patterns formed are defined as a combination of single vortices and vortex pairs shed over one cycle. The 2S wake mode consists of two single vortices of opposite sign shed over one cylinder oscillation cycle. The 2P wake mode consists of two counter-rotating pairs of vortices shed per cylinder oscillation cycle. The P + S wake mode consists of a vortex pair and a single vortex shed per cylinder oscillation cycle. The 2P + 2S mode consists of two counter-rotating pairs of vortices shed per cylinder oscillation cycle along with a single vortex shed between each pair. The P and 2P* wake modes are asymmetric modes convecting to one side, with the side selected based on the history of the flow. They also observed vortex coalescence, the phenomenon of vortex merging, with vortices of the same sense merging (coalescing) together to form larger vortical structures. A slightly modified version of this wake mode classification scheme is used in the present study.

While there are numerous studies on flow around cylinders oscillating in transverse or streamwise directions, comparatively fewer studies exist on vortex shedding from cylinders undergoing rotary oscillations. Experimental studies have been performed by Tokumaru & Dimotakis (1991), Fujisawa, Kawaji & Ikemoto (2001), Fujisawa, Tanahashi & Srinivas (2005), Lee & Lee (2006), Saad, Lee & Lee (2007), Lee & Lee (2008), Nazarinia *et al.* (2012) and, most recently, Kumar *et al.* (2013)

https://doi.org/10.1017/jfm.2014.191 Published online by Cambridge University Press

and Sellappan & Pottebaum (2014). Tokumaru & Dimotakis (1991) conducted an experimental study at $Re = 15\,000$, performing flow visualization and wake profile measurements on circular cylinders undergoing forced rotary oscillations in a steady uniform flow and found that the drag forces on the cylinder were reduced at high oscillation frequencies while undergoing rotary forcing. Fujisawa *et al.* (2001) looked at methods for controlling vortex shedding from circular cylinders using rotary oscillations at $Re = 6700$ and $Re = 20\,000$ and found that active flow control was feasible under certain forcing conditions. Fujisawa *et al.* (2005) carried out a study which combined numerical techniques with experimental data obtained using particle image velocimetry (PIV) and found that at $Re = 2000$ drag force on a cylinder undergoing rotary oscillations is dependent on forcing frequencies. One study that looked at the behaviour of both stationary and rotationally oscillating cylinders was by Saad *et al.* (2007), with the oscillating cylinder experiments performed at $Re = 3700$, and comparisons were made between the wake of an unforced and forced cylinder and it was also shown that the formation length decreased with increasing frequency of rotary oscillations. Recently, Kumar *et al.* (2013) experimentally studied vortex shedding from rotationally oscillating cylinders at $Re = 185$ using the hydrogen bubble technique, hot-wire anemometry and PIV and identified the oscillation conditions under which the shedding is synchronized to the forcing. They also studied the possibility of forcing the wake to become two-dimensional through rotary forcing at $Re = 185$ and $Re = 400$ and identified forcing conditions under which it is possible to do so. One experimental study that looked at a slightly different forcing configuration was by Nazarinia *et al.* (2012). They studied cylinders in a uniform flow at $Re = 1322$ undergoing combined rotary and translational forcing and found wake modes similar to those observed for cylinders undergoing rotary forcing only. They also found both synchronized and unlocked near-wake structures depending on the frequency ratio between the translational and rotational motions.

Studies that have numerically investigated the flow around rotationally oscillating cylinders include Lu & Sato (1996), Baek & Sung (2000), Dennis, Nguyen & Kocabiyik (2000), He *et al.* (2000), Mahfouz & Badr (2000*a*), Lo Jacono *et al.* (2010), Lu *et al.* (2011) and Du & Dalton (2013), among others. One early study was by Lu & Sato (1996) in which the authors looked at flow past rotationally oscillating cylinders at three different Re (200, 1000, 3000) with frequency ratios ranging up to four times the natural shedding frequency. They obtained the basic flow structure at certain forcing conditions and measured the influence of cylinder forcing on the lift and drag forces acting on the cylinder. Most interestingly, they were also able to sketch a vortex mode-selection diagram which showed the primary lock-on region around the natural shedding frequency. Similar synchronized wake structures were also observed by Baek & Sung (2000) in direct numerical simulations of the wake of a rotationally oscillating cylinder at $Re = 110$. They performed detailed numerical analyses and obtained the stability characteristics of the wake and also identified 'lock-on' and 'non-lock-on' states of the wake when the cylinder is rotationally forced. Stability characteristics of the wake and the transition to three-dimensional flow have also been studied through Floquet stability analysis (Lo Jacono *et al.* 2010). They found that, for a rotationally oscillating cylinder at $Re = 300$, mode B instabilities are suppressed at high amplitudes of rotation, but predicted that it might be possible for the flow to transition due to another type of instability (mode D). They also observed that the near-wake was locked-on to the cylinder forcing. The vortex shedding patterns and the dependence of lift and drag forces on rotary forcing were also studied by Dennis *et al.* (2000) who looked at an impulsively

https://doi.org/10.1017/jfm.2014.191 Published online by Cambridge University Press

started cylinder translating with a constant velocity in a direction normal to the cylinder axis while performing rotational oscillations at $Re = 500$ and $Re = 1000$. They observed a reduction in drag forces with increase in oscillation frequencies under certain conditions, similar to Tokumaru & Dimotakis (1991), but found that vortex shedding patterns in the near-wake of forced cylinders did not match with the results of Lu & Sato (1996) for certain flow conditions. Other numerical studies that have observed reduced forces on the cylinder due to rotary forcing include He *et al.* (2000), who found significant drag reduction for flows in the range $200 \leqslant Re \leqslant 1000$, Lu *et al.* (2011), who found reduced lift and drag forces at low Reynolds numbers ($Re = 60$, 80, 100, 150, 200), and Du & Dalton (2013), who performed two- and three-dimensional computations at $Re = 150$ and $Re = 15\,000$, respectively, and found varying amounts of drag reduction. At the higher Re, Du & Dalton (2013) observed a drag reduction trend similar to the experimental results of Tokumaru & Dimotakis (1991).

Mahfouz & Badr (2000*a*) numerically investigated the flow in the wake of a circular cylinder performing rotational oscillation about its own axis. They studied flows up to a Reynolds number of 200 and forcing frequencies up to two times the natural shedding frequency. They found the lock-on phenomenon, in which the frequency of vortex shedding is 'locked-on' or synchronized with the forcing frequency, to occur within a narrow region of the parameter space around the natural shedding frequency. They predict the frequency range over which this lock-on occurs to increase with the amplitude of oscillation and also predict a threshold value below which this frequency range is zero. At oscillation amplitudes below the threshold value the shedding is locked on only for $F_R = 1.0$. Similar results were obtained by Lee & Lee (2006). They conducted experiments with forcing frequencies up to two times the natural shedding frequency and found locked-on wake structures in the wake of a rotationally oscillating cylinder at $Re = 4140$. Further detailed PIV measurements of the near-wake when the cylinder is forced with an oscillation amplitude $\theta_{PP} = 1.04$ and frequency ratios $F_R = 0.4$, 0.8, 1.0, 1.6 at $Re = 4140$ were given by Lee & Lee (2008). They also found the wake to be locked-on to the forcing when $F_R = 1.0$, but observed only a transition regime when $F_R = 0.8$, 1.6 and a non-lock-on regime when $F_R = 0.4$. Most recently, Sellappan & Pottebaum (2014) showed experimentally that locked-on wake modes occur over a large range of forcing conditions for rotationally oscillating cylinders at $Re = 150$, including wake modes synchronized over multiple cylinder oscillation cycles. Wake mode boundaries identified by some of these authors are shown in figure 3. The locations of the mode boundaries in the $\theta_{PP} - F_R$ parameter space are approximate. In the case of data from Lee & Lee (2008), the lock-on boundaries are drawn such that they are approximately equidistant between the locked-on data point at $F_R = 1.0$ and the transition regime data points on either side. The existence of the primary lock-on region centred around the Strouhal frequency for different values of Re is apparent from figure 3.

Thiria, Goujon-Durand & Wesfreid (2006) and Thiria & Wesfreid (2007) also observed similar phenomena. They described the shedding as 'non-lock-on' if the spectra contains complex frequency content that includes the forcing frequency and a frequency linked to the far-wake instability. They explained the 'non-lock-on' regime as being caused due to far-wake instabilities and identified boundaries between lock-on and non-lock-on regions. In Sellappan & Pottebaum (2014) and in the present study, it was observed that this kind of mixed frequency content is actually indicative of a transition between lock-on and a total non-lock-on regime in which the forcing frequency is almost completely absent from the spectra. Thiria & Wesfreid (2007)

https://doi.org/10.1017/jfm.2014.191 Published online by Cambridge University Press

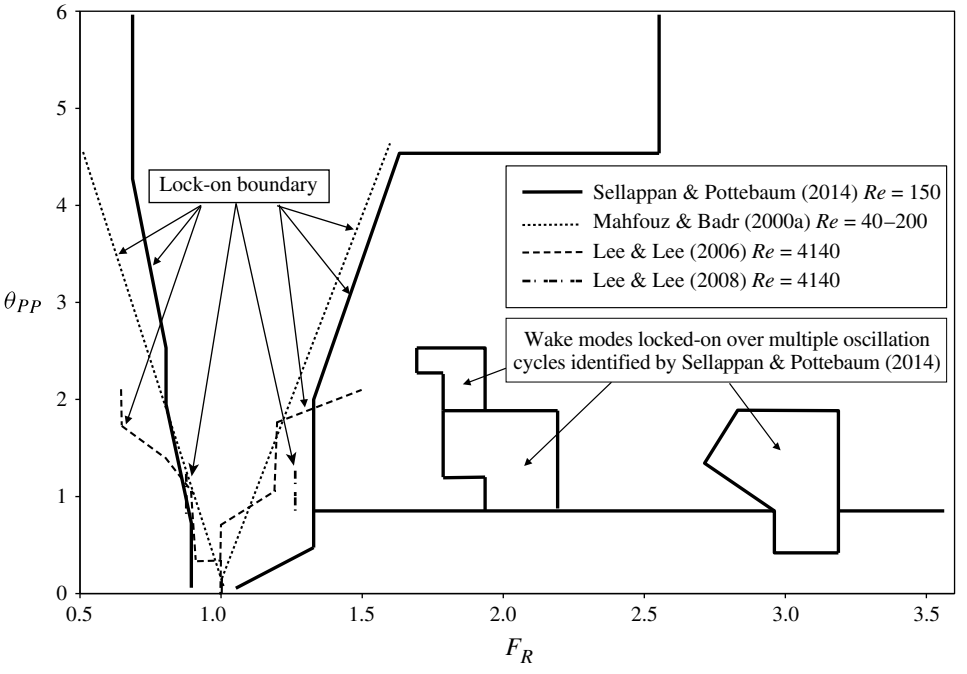


FIGURE 3. Wake mode boundaries (approximate) identified by various authors at different *Re* for a rotationally oscillating cylinder.

applied linear stability analysis to a time-averaged mean flow at $Re = 150$ and obtained the stability properties by numerical solution of the inviscid Orr–Sommerfeld equation and showed that it can account for the stability properties of the wake even under rotary forcing conditions. They showed that the wake exhibits a finite region of absolute instability immediately behind the cylinder and this region transitions to a region of convective instability and explained the presence of the lock-on region by showing that it is reached when cylinder forcing conditions trigger the transition to convective instability. They also observed that under certain forcing conditions the vortices shed from the cylinder coalesce to form larger vortical structures. This coalescence phenomena was also observed in the present study.

1.2. *Heat transfer from cylinders*

Heat transfer from stationary cylinders in cross-flow has been studied extensively and the basic mechanism is considered well understood and information on this can be found in any standard textbook on heat transfer such as Incropera & Dewitt (1996) and reviews of existing studies and empirical correlations for heat-transfer coefficients can be found in Morgan (1975) and Sparrow, Abraham & Tong (2004). Sparrow *et al.* (2004) also present an exhaustive collection of published data on heat-transfer coefficients for non-circular and circular cylinders and for spheres in cross-flow, while detailed information on convective heat transfer from smooth circular cylinders is available in Morgan (1975). A review of previous numerical studies can be found in Bouhairie & Chu (2007). The numerical simulation by Bouhairie & Chu (2007) looked at heat transfer from a circular cylinder into a cross-flow for $Re = 200$–$15\,550$. They computed the unsteady heat transfer using a two-dimensional

https://doi.org/10.1017/jfm.2014.191 Published online by Cambridge University Press

model which simulated the local and overall heat-transfer rates. It should be noted that there are intrinsic flow instabilities in the range of Re they studied that might render the flow three-dimensional and two-dimensional simulations may not be able to fully capture these effects. A study by Chang & Mills (2004) looked at the effect of aspect ratio on heat transfer to cylinders in a cross-flow with Re ranging between 6300–50 960. Even in the small range of aspect ratios, $6 \leqslant AR \leqslant 12$, tested, it was shown that circumferentially averaged and total averaged Nusselt numbers increased with decreasing aspect ratio. There have been many experimental studies which provide empirical correlations between the heat-transfer rate and Reynolds number. Through these studies, it has been shown that heat transfer from a cylinder placed in cross-flow consists of two steps. In the first step, heat is transferred from the cylinder onto the viscous boundary layer through conduction. In the second step, the fluid entrained in the boundary layer is then removed through the alternate shedding of vortices. Therefore, in the case of a cylinder, heat-transfer enhancement depends on enhancing the removal of fluid from the 'dead-water' region downstream of the cylinder. This can be accomplished by cylinder forcing.

Heat transfer from cylinders undergoing forced oscillations has been studied for a long time. One of the earliest studies was by Sreenivasan & Ramachandran (1961). They looked at heat transfer from cylinders undergoing transverse oscillations in the range $2500 \leqslant Re \leqslant 15\,000$ and found no appreciable increase in the heat-transfer rate. Recently, Pottebaum (2003) and Pottebaum & Gharib (2006) showed that transversely forced cylinders in a cross-flow do exhibit significant heat-transfer enhancement under certain forcing conditions. They also explained the lack of heat-transfer enhancement seen by Sreenivasan & Ramachandran (1961) to be due to the low-frequency ratios studied. The study by Pottebaum & Gharib (2006) was done at $Re = 687$ and they showed that the heat transfer is significantly enhanced by small-amplitude oscillations at frequencies near the Strouhal frequency and its harmonics. Heat transfer from cylinders undergoing rotary oscillations has been studied recently by Mahfouz & Badr (2000*b*). Their numerical study looked at flows between $40 \leqslant Re \leqslant 200$. The frequency ratios considered were $0 \leqslant F_R \leqslant 2$. They found that the vortex shedding influences the thermal field in the wake region and observed significant heat-transfer enhancement in the lock-on region. However, the effect of wake structures synchronized over multiple oscillation cycles and its relationship with heat-transfer enhancement was not studied.

Very little is known about the effect of harmonics on the heat-transfer rate from rotationally oscillating cylinders and changes, if any, in the wake structure that are produced due to heating the cylinder. Therefore, a comprehensive study of the relationship between wake formation and heat transfer from rotationally oscillating cylinders is required. In the current study, results of experiments to study changes produced in the wake structure by rotary cylinder forcing and the effect of the wake structure on convective heat transfer are described.

2. Experimental details

2.1. *Experimental set-up*

The experiments were performed in a water tunnel designed for constant free-stream temperature conditions. The test section of the water tunnel is made of Plexiglas, to allow for visual observation, and is 0.152 m wide, 0.58 m long and has a maximum height of 0.16 m. For all of the experiments the water depth was maintained at 0.137 m and the top surface was not covered and had a stable free surface. Due to the relatively small cross-sectional area the blockage effect speeds up the flow in the

https://doi.org/10.1017/jfm.2014.191 Published online by Cambridge University Press

boundary layer region leading to slightly higher effective Re. The upstream section of the water tunnel contained a honeycomb structure, multiple meshes with increasing mesh density and, finally, a convergent section leading to the test section, to create a uniform flow at the cylinder location. The flow speed U_0 at the cylinder location in the test section was maintained at 0.0698 ± 0.0002 m s^{-1}, and the turbulence intensity at the location of the cylinder in the test section was found to be around 0.3 % under experimental conditions. The incoming flow velocity was measured using digital particle image velocimetry (DPIV) and was found to vary less than $\sim$1.5 % in the middle 25 % of the channel width and height near the cylinder location in the test section. For all of the experiments discussed in this study the free-stream temperature, T_∞, of the tunnel was maintained at $25.8 \pm 0.2\,^{\circ}$C. A circular cylinder (Watlow custom cartridge heater) having a diameter D of 0.009 42 m was used in the experiments and was submerged to a depth L of 0.13 m, normal to the flow direction and to the bottom wall of the water tunnel, with the lower end of the cylinder suspended 7 mm above the bottom wall. This translates to an cylinder aspect ratio of 13.8 and test section blockage ratio of 0.0620. The upper end of the cylinder extends out of the free surface of the water in the channel and is attached to a custom built cylinder mount. The cylinder was oscillated with a sinusoidal rotary motion, $\theta(t) = (\theta_{PP}/2)\,\sin(2\pi f_f t)$, about its own axis. The cylinder motion was controlled using a closed-loop motion control system. The major components of the motion control system were a stepper motor with 0.225° resolution (Anaheim Automation 23MD006D-10-00-00), a rotary optical encoder (US Digital E2-1000-250-I-H-G-3), a multifunction data acquisition board (National Instruments PCI-6229), and custom motion control program. Motion profiles were specified such that the cylinder motion was smooth and there were no 'stop-and-go' movements. The time between successive points on the profile never exceeded 0.5 % of the cylinder forcing period and the forcing amplitude had an uncertainty of 2.2 % for the smallest forcing amplitude studied. The range of cylinder oscillation conditions studied were $0.09 \leqslant \theta_{PP} \leqslant 2.09$ and $0.70 \leqslant F_R \leqslant 3.16$. The kinematic viscosity of water at the experiment free-stream temperature, $\nu = 8.77 \times 10^{-7}$ m^2 s^{-1}, translates to a Reynolds number $Re = 750 \pm 4$.

Under these conditions, the question then arises as to the two-dimensionality of the flow and end effects due to the relatively small aspect ratio. It is a well-known result that the wake of a stationary cylinder transitions to a three-dimensional regime for $Re \approx 190$ (Williamson 1996), with mode B structures being the dominant form at $Re = 750$. Williamson (1989) showed that for relatively small aspect ratios, such as in the current set-up, the vortex shedding from a stationary cylinder is oblique and not parallel. In the current set-up, there are no end plates and the shedding when the cylinder is stationary is assumed to be oblique due to end effects. However, it has been shown that rotationally oscillating the cylinder suppresses instabilities, thereby bringing the flow back to a nominally two-dimensional state (Poncet 2002; Jian, Xue-ming & An-lu 2007; Kumar *et al.* 2013). In particular, Kumar *et al.* (2013), through an extremely well-designed set of experiments using the hydrogen bubble technique and utilizing a unique end view perspective of the wake structure, have shown that rotary oscillations are capable of bringing the shedding back to a nominally two-dimensional state under certain forcing conditions even for relatively small-aspect-ratio cylinders at moderately high Re. Evidence in favour of two-dimensionality was obtained during the set up and testing phase of the present study as the wake was measured at different spanwise locations. The mean wake profile and wake modes were found to be similar at spanwise locations located at mid-span and $\sim 0.75D$ above and below mid-span, as would be expected if the rotary

https://doi.org/10.1017/jfm.2014.191 Published online by Cambridge University Press

forcing aligned the shedding with the cylinder. Based on these results, and the results of Poncet (2002), Jian *et al.* (2007) and Kumar *et al.* (2013), it is reasonable to speculate that the shedding is parallel and nominally two-dimensional everywhere along the span of the cylinder, except very close to the boundaries due to end effects. This does not exclude the possible existence of small-scale three-dimensional structures that have not been captured due to experimental limitations.

Two sets of experiments, a parameter space survey to determine heat-transfer rates for a large number of cases and, then, a detailed study of the wake structure of a few select cases using DPIV, were performed. During the parameter space survey, a total of 357 cases were tested to measure the rate of heat transfer from a heated cylinder to the ambient fluid and its dependence on forcing conditions. In the second set of experiments, both heated and unheated cylinders were studied using DPIV. In the second set, the cylinder was initially not heated and only wake structure information was obtained using DPIV at 177 different cylinder oscillation conditions. Next, the cylinder was heated with a constant power input and 114 distinct oscillation conditions were tested and both heat-transfer information and wake information was obtained concurrently.

2.2. *Heat-transfer experiments*

For all heat-transfer experiments, heating power was provided by a variable-voltage DC power supply unit (Agilent E3648A) to a heating coil embedded in the cylinder. It consists of a thin coil of high resistivity wire (80 % Ni, 20 % Cr) surrounded by compacted magnesium oxide insulator and encased in an Incolloy® 800 (a stainless steel alloy) sheath. The cylinder mount was made of an insulating material to prevent heat loss through conduction. The heated length of the cylinder was submerged in the flow and a nominal input power, P_{in}, of 59.26 ± 0.02 W was supplied and the actual power input independently monitored. This level of power input was chosen because it generates temperature differences in the flow that are measurable but do not cause significant buoyancy forces. The Richardson number, defined as the ratio of buoyancy forces to inertial forces in the vertical momentum equation, $Ri = gD\beta\Delta T/U_0^2$, where g is gravitational acceleration, β is the volumetric coefficient of thermal expansion for water, ΔT is the difference between the cylinder surface temperature and the free-stream temperature, was maintained below 0.05 in order to ensure that forced convection was dominant. Another important parameter is the ratio of momentum diffusivity to thermal diffusivity, namely, Prandtl number, $Pr = \nu/\alpha$. For this experiment, $Pr = 6.0$. The heat-transfer coefficient, h, for the cylinder was calculated from the temperature at the cylinder core, T_{tc}, which was measured using an embedded type-J thermocouple. The leads of this thermocouple were connected to a signal conditioner (Omega SMCJ-J) which converted the thermocouple signal to a cold junction compensated, linear, amplified analogue signal that was recorded using a data acquisition device (National Instruments PCI-6229) and custom LabVIEW program. The heat-transfer coefficient was calculated by assuming a steady, one-dimensional model of heat transfer inside the cylinder. Based on this model, the resulting expression for the heat-transfer coefficient, h, is, $h = ((2\pi(D/2)L(T_{tc} - T_\infty)/P_{in}) + C_{\Delta T})^{-1}$, where $C_{\Delta T}$ is a constant of proportionality that depends only on the cylinder dimensions and material properties. Further details of the cylinder geometry, heat-transfer model, determination of the heat-transfer coefficient and a comprehensive error analysis are available in the literature (Pottebaum 2003; Pottebaum & Gharib 2006; Sellappan 2013, § 2.6). The

https://doi.org/10.1017/jfm.2014.191 Published online by Cambridge University Press

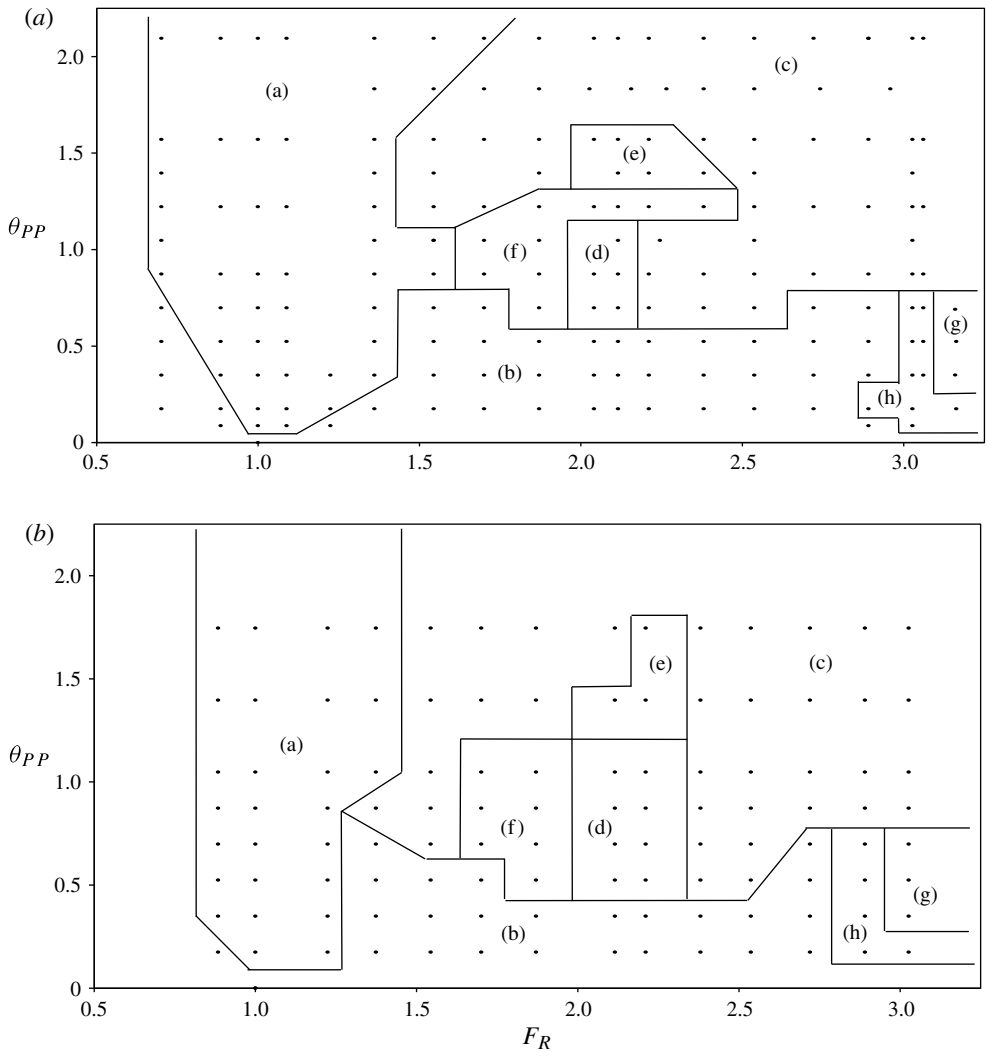


FIGURE 4. Map of wake mode regions for (*a*) an unheated cylinder and (*b*) a heated cylinder. Solid lines represent approximate wake mode boundaries and dots represent cases studied using DPIV. Wake mode regions: (a) 2S lock-on region; (b) non-lock-on region; (c) near-wake 2S, far-wake non-locked-on; (d) (1/2)(2S) far-wake mode; (e) (1/2)(P + S) far-wake mode; (f) (1/2)(P + S), no coalescence; (g) (1/3)(P + S), no coalescence; (h) (1/3)(2P), no coalescence.

heat-transfer coefficient obtained using this method is then normalized as the Nusselt number, $Nu = hD/k$, where k is the thermal conductivity of the fluid. The main source of uncertainty is in the measurement of the cylinder core temperature, T_{tc}, measured using a thermocouple which was uncertain within $\pm 0.1\,^{\circ}\mathrm{C}$. For all cases, thermocouple data was recorded for a period of 120 s. This was done to ensure that, for any given oscillation condition, data over a large number of oscillation cycles were captured. A 45 s delay was imposed before data recording to allow for any transient effects to die out.

https://doi.org/10.1017/jfm.2014.191 Published online by Cambridge University Press

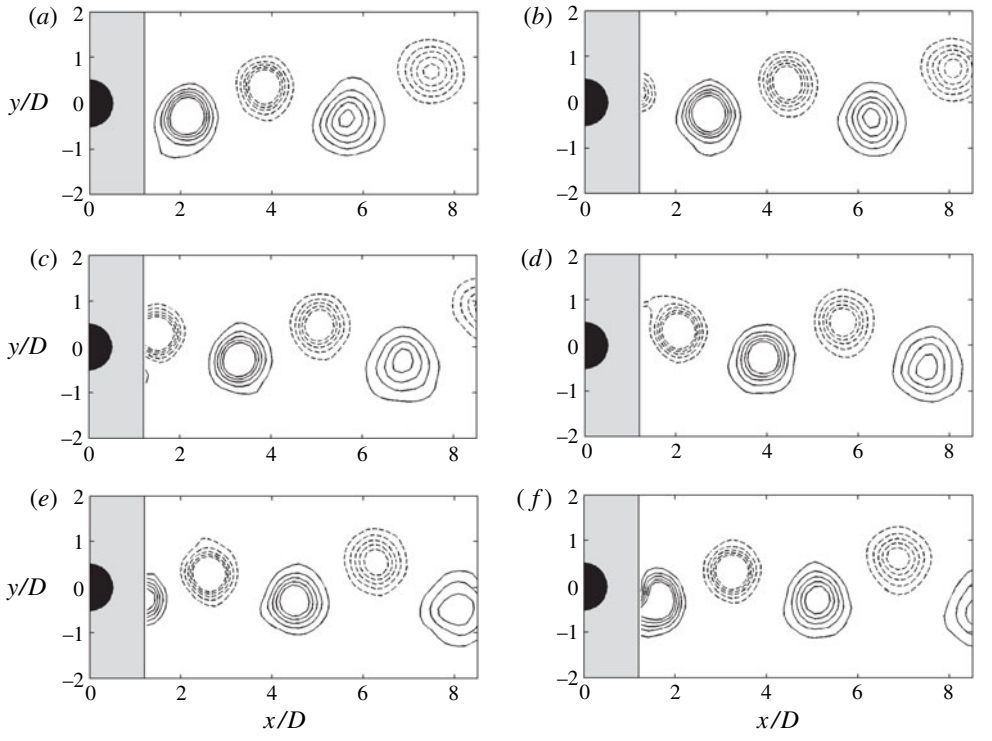


FIGURE 5. Phase-averaged Ω for an unheated cylinder. Cylinder forced at $\theta_{PP} = 2.09$, $F_R = 1.0$. Phase averaged over one oscillation cycle: (*a*) $\Phi = 0$; (*b*) $\Phi = \pi/3$; (*c*) $\Phi = 2\pi/3$; (*d*) $\Phi = \pi$; (*e*) $\Phi = 4\pi/3$; and (*f*) $\Phi = 5\pi/3$.

2.3. *Digital particle image velocimetry*

Velocity data were obtained using DPIV. The water tunnel was seeded using silver-coated, hollow, glass spheres (Potters Industries CONDUCT-O-FIL SH400S33) with an average particle diameter of 14×10^{-6} m and average density of 1700 kg m^{-3}. The particles were illuminated by a horizontal laser sheet with a wavelength of 532 nm emitted by a pulsed laser system (NEW WAVE Research Solo III). The laser sheet had a thickness of $\sim$5 mm at the mid-plane of the test section and was located at a height of 0.065 m above the bottom wall. The thickness of the laser sheet used in the present study is slightly larger than that used in other studies and its effect on the measurements is not straightforward. While it increases the measurement uncertainty due to magnification errors, which are minimized to an extent by the use of a long focal length in the camera optics, the relatively thicker laser sheet also reduces the particle drop-out rate caused by out-of-plane motion between frames. This reduction in particle losses between frames reduces the measurement uncertainty. This DPIV system has been used by the authors in previous studies such as Sellappan (2013) and Sellappan & Pottebaum (2014) and the velocity measurements made using this set-up have relative uncertainties of 1.5–3 %. For all test cases presented here, 3500 images (1750 image pairs) with image resolution of 1024×768 pixels were acquired at 27 f.p.s. and were recorded using a black and white, CCD camera (Sony XCL X-700) connected to a frame grabber (Dalsa-Coreco X64-CL Express). Since the cylinder used in the experiment is not transparent and the laser sheet originates from a point

https://doi.org/10.1017/jfm.2014.191 Published online by Cambridge University Press

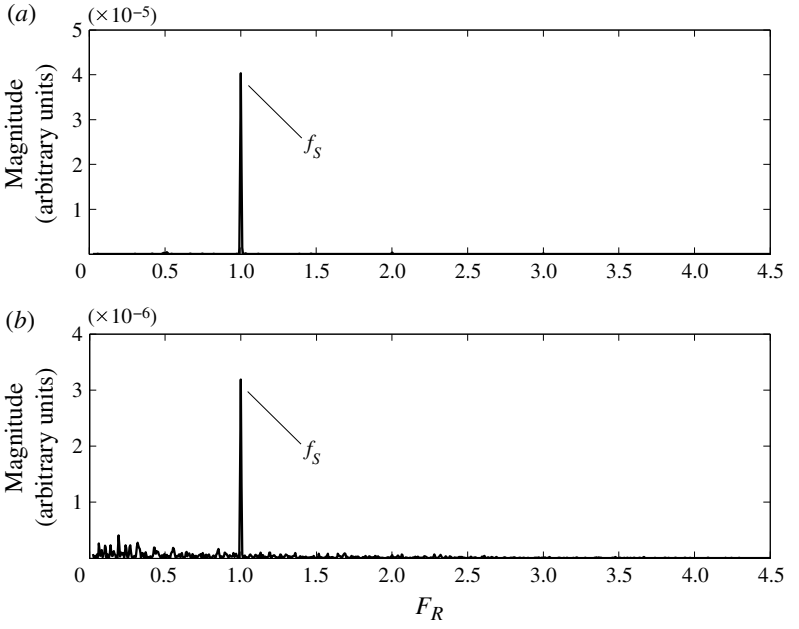


FIGURE 6. Spectra measured along $y/D = -0.01$ at streamwise locations (*a*) $x/D = 1.71$ and (*b*) $x/D = 7.77$. Cylinder is unheated. Cylinder forced at $\theta_{PP} = 2.09$, $F_R = 1.0$.

that is located such that the azimuthal angle formed with respect to the centre of the cylinder and the upstream stagnation point is less than 90° the cylinder casts a shadow downstream of the cylinder and all images contain a shadow, and no velocity information can be obtained from the shadow region. The area imaged by the camera was set in such a way that the downstream half of the cylinder was always present in the image, and the wake region imaged varied in length from 5 to 10 cylinder diameters, with most cases having an imaged area of $\sim 7D \times 4D$. This leads to a scale of ~ 0.06 mm pixel^{-1}. The recorded images were processed and post-processed, after excluding the shadow region, for each case using standard DPIV algorithms with 32×32 pixels interrogation windows and 50 % overlap, and velocity fields with 54×43 vectors and a spatial resolution of $\sim 0.13D$ were calculated. From the velocity vectors, the out-of-plane component of vorticity, ω_z, was calculated.

2.4. *Spectral analysis*

Spectral analysis of velocity data is used to measure the frequency of the vortex shedding and to detect the presence of any harmonics or the cylinder forcing frequency in the wake. The presence of only the forcing frequency as the dominant frequency in the power spectrum is an indication of the lock-on phenomenon. Presence of peaks in the power spectrum, at the forcing frequency and also the natural shedding frequency, is an indication of a transition regime. The presence of the natural shedding frequency as the dominant frequency and the absence of the forcing frequency in the power spectrum indicates that vortex shedding is not locked to the forcing of the cylinder. Spectral analysis is performed by extracting the time series of the streamwise velocity component in the DPIV data at multiple locations in the spatial domain downstream of the cylinder. A Hanning windowing function was applied to

https://doi.org/10.1017/jfm.2014.191 Published online by Cambridge University Press

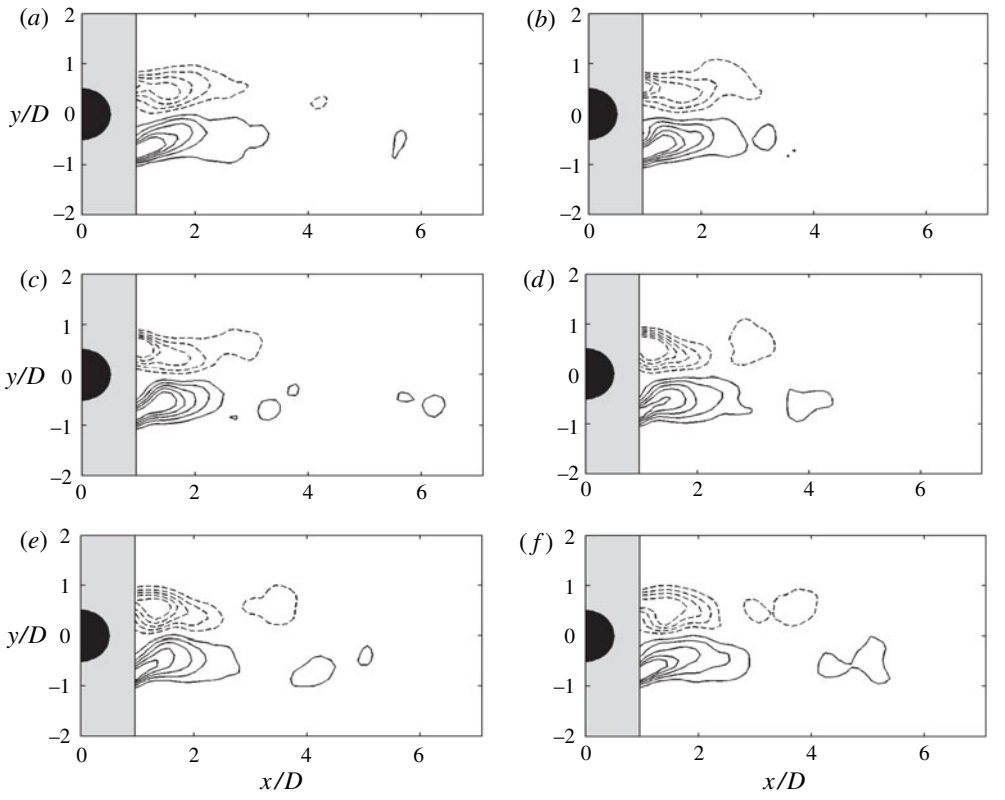


FIGURE 7. Phase-averaged Ω for an unheated cylinder. Cylinder forced at $\theta_{PP} = 0.17$, $F_R = 1.87$. Phase averaged over one oscillation cycle: (*a*) $\Phi = 0$; (*b*) $\Phi = \pi/3$; (*c*) $\Phi = 2\pi/3$; (*d*) $\Phi = \pi$; (*e*) $\Phi = 4\pi/3$; and (*f*) $\Phi = 5\pi/3$.

the data and power spectra were calculated. For all cases, each time series signal extracted from the DPIV velocity data had 1750 data points (equal to the number of DPIV velocity fields) obtained at an effective sampling frequency of 13.5 Hz (acquisition rate of image pairs). The Strouhal frequency, $f_S = 1.47$ Hz, was obtained by spectral analysis of the time series of the x-component of velocity at various locations in the wake of a stationary cylinder and the Strouhal number was estimated to be $St = 0.198$, uncertain within $\sim 3\,\%$, for both heated and unheated cylinders. For heated stationary cylinders, experiments by Hu & Koochesfahani (2011) at $Re = 135$ have shown that the Strouhal number depends on the Richardson number, with St decreasing dramatically for $Ri \geqslant 0.31$, but exhibiting only a moderate decrease for $Ri < 0.31$. Vit *et al.* (2007) found that, at low Re ($Re \leqslant 90$), the Strouhal number increased for increasing values of Ri (for $Ri \leqslant 0.15$). The contradictory results are due to the fact that both experiments were performed in different flow configurations and convection regimes. No changes in St due to heating of the cylinder were observed in the present study, which could be due to the different flow configuration (direction of incoming free-stream flow relative to the direction of buoyancy forces), or the significantly lower Ri, and/or the higher Re regime. No effort was made in the present study, such as increasing the Ri, to ascertain whether the trends seen by Hu & Koochesfahani (2011) or Vit *et al.* (2007) also occur at the present experimental conditions.

https://doi.org/10.1017/jfm.2014.191 Published online by Cambridge University Press

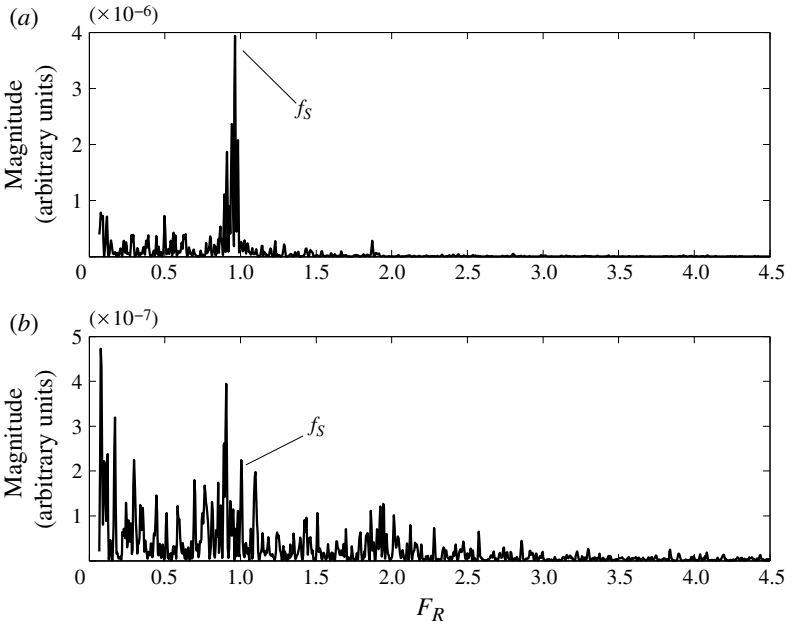


FIGURE 8. Spectra measured along $y/D = -0.02$ at streamwise locations (*a*) $x/D = 1.32$ and (*b*) $x/D = 4.83$. Cylinder is unheated. Cylinder forced at $\theta_{PP} = 0.17$, $F_R = 1.87$.

2.5. *Phase averaging*

Background noise and cycle-to-cycle variations are two factors that lead to difficulty in identifying wake structures in the vorticity data. To overcome this, vorticity fields calculated from the DPIV data are phase averaged. This is accomplished by calculating the phase of each vorticity field obtained from the DPIV data. This is done using the known cylinder oscillation frequency and the time between image pairs and grouping vorticity fields into bins of equal width on the basis of their phase, ϕ. The vorticity fields in each bin are then averaged. Phase averaging was also done over multiple cylinder oscillation cycles to study vorticity structures that are in-phase over multiple cycles. Therefore, for every case, phase averaging was done over one, two and three cylinder oscillation cycles.

3. Results and discussion

3.1. *Wake modes of heated and unheated cylinders*

In order to understand wake formation and its dependence on forcing conditions and heat transfer, experiments were performed with the cylinder both heated and unheated. In comparing heated with unheated conditions, it was clear that heating the cylinder resulted in the formation of the same wake modes as those present in the wake of an unheated cylinder. Heating the cylinder was found to change the shape of wake mode regions and location of wake mode boundaries. Due to constraints of space, for each unique wake mode region, only a single set of plots, either for a heated cylinder or a unheated cylinder, of phase-averaged normalized vorticity and power spectra are shown in this paper. For both the heated and unheated cylinders, the vorticity fields and power spectra are qualitatively similar for all cases within the same wake mode region. The full results of these experiments are available in Sellappan (2013). A map

https://doi.org/10.1017/jfm.2014.191 Published online by Cambridge University Press

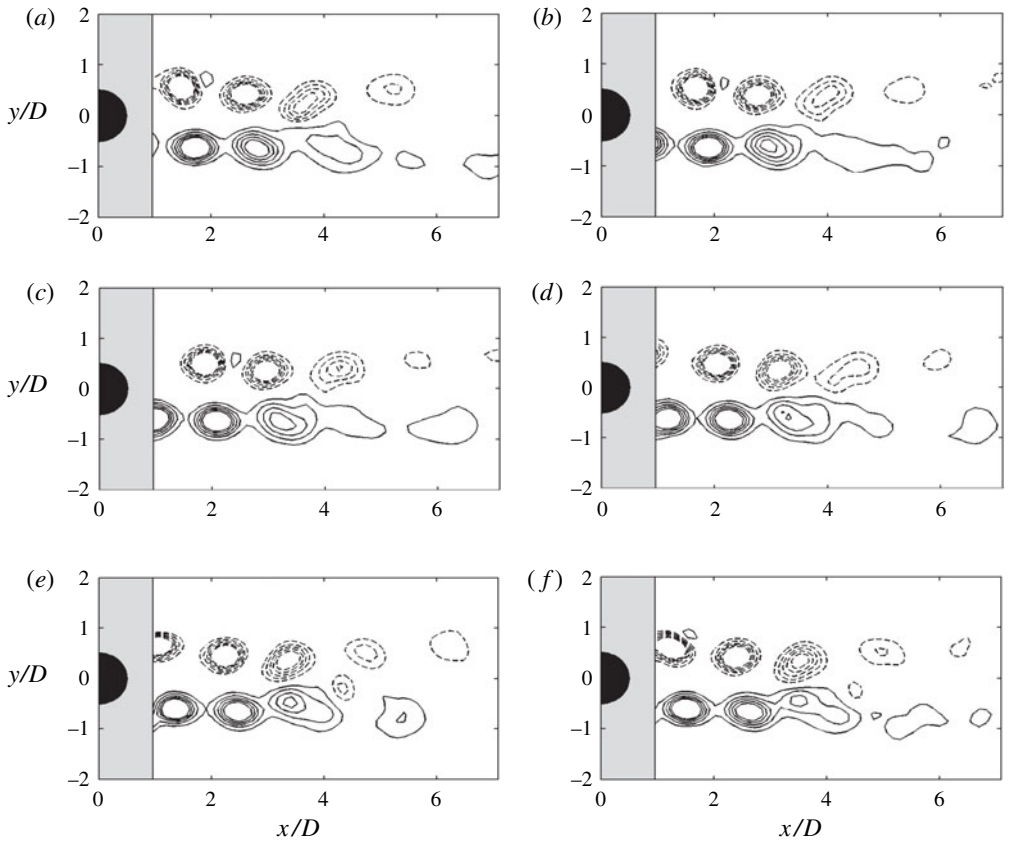


FIGURE 9. Phase-averaged Ω for a heated cylinder: (*a*) $\Phi = 0$; (*b*) $\Phi = \pi/3$; (*c*) $\Phi = 2\pi/3$; (*d*) $\Phi = \pi$; (*e*) $\Phi = 4\pi/3$; and (*f*) $\Phi = 5\pi/3$. Cylinder forced at $\theta_{PP} = 1.40$, $F_R = 2.72$. Phase averaged over one oscillation cycle.

of wake mode regions identified for the unheated cylinder is given in figure 4(*a*) and for the heated cylinder in figure 4(*b*).

At higher forcing frequencies, coalescence (merging of vortices of the same sense) is observed in certain areas of the parameter space, but not all. In cases that exhibit coalescence, spectral analysis of the wake at locations downstream of the coalescence location shows that the dominant frequencies in the power spectrum are different from the frequencies observed before coalescence. The portion of the wake immediately downstream of the cylinder and extending up to the coalescence location is classified as near-wake and the wake downstream of the coalescence location is classified as far-wake. Coalescence is the mechanism by which a less-stable wake configuration transitions to a more stable one. When the near-wake is unstable, it transitions to a different wake structure through the combination of smaller vortices to form larger vortical structures which are arranged in a globally stable formation. This stable far-wake is usually similar to the wake of an unforced cylinder, but other stable arrangements are also possible under certain conditions, depending on the cylinder forcing and the unperturbed outer flow.

All vorticity fields presented in the results of this paper are shown as contour plots of normalized vorticity, $\Omega = \omega_z D/U_0$, phase-averaged over one, two, or three

https://doi.org/10.1017/jfm.2014.191 Published online by Cambridge University Press

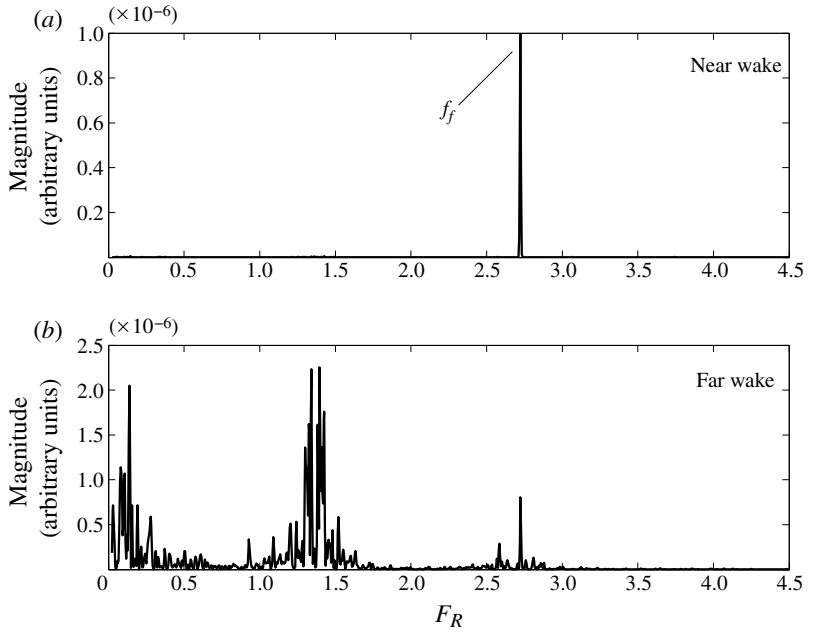


FIGURE 10. Spectra measured along $y/D = -0.26$ at streamwise locations (*a*) $x/D = 1.79$ and (*b*) $x/D = 4.13$. Cylinder is heated. Cylinder forced at $\theta_{PP} = 1.40$, $F_R = 2.72$.

oscillation cycles, with minimum contour levels at ± 0.5 and contour spacing of 0.5. Positive contours are shown as solid lines, and negative contours are shown as dashed lines.

3.1.1. *Wake modes at forcing frequencies near the natural shedding frequency*

When the cylinder was forced at frequencies close to the natural shedding frequency, the lock-on phenomenon occurred as expected. This lock-on phenomenon occurred in the wake of the cylinder both when it was heated and also when it was unheated, but there were certain differences in the range and shape of this region in the parameter space for the two conditions. In figure 4, the primary lock-on region, region (*a*), is labelled as '2S lock-on region, no coalescence'. It is apparent that the lock-on region is narrower for the heated cylinder, compared with the unheated cylinder. In both cases, the frequency range over which lock-on occurs is found to increase with increase in oscillation amplitude but the increase is not uniform. The unheated cylinder shows a steeper increase, which becomes more pronounced for $\theta_{PP} > \pi/2$. When the forcing frequency was equal to the Strouhal frequency ($F_R = 1.0$), both the unheated and heated cylinder have lock-on even at the lowest amplitudes that were studied. Figure 5 shows the phase-averaged vorticity fields seen in the wake of an unheated cylinder for the locked-on case, $\theta_{PP} = 2.09$ and $F_R = 1.00$, and figure 6 shows the power spectra for the same case. The vorticity fields are phase-averaged over one cylinder oscillation cycle and two vortices, one of each sign, are shed per cycle. Therefore, it is classified as a 2S wake mode. The power spectra show only one dominant frequency, at the forcing frequency f_f, which is also equal to f_S since $F_R = 1.0$. The presence of only the forcing frequency as the dominant frequency is an indication that the shedding is locked on to the cylinder forcing. This dominance is

https://doi.org/10.1017/jfm.2014.191 Published online by Cambridge University Press

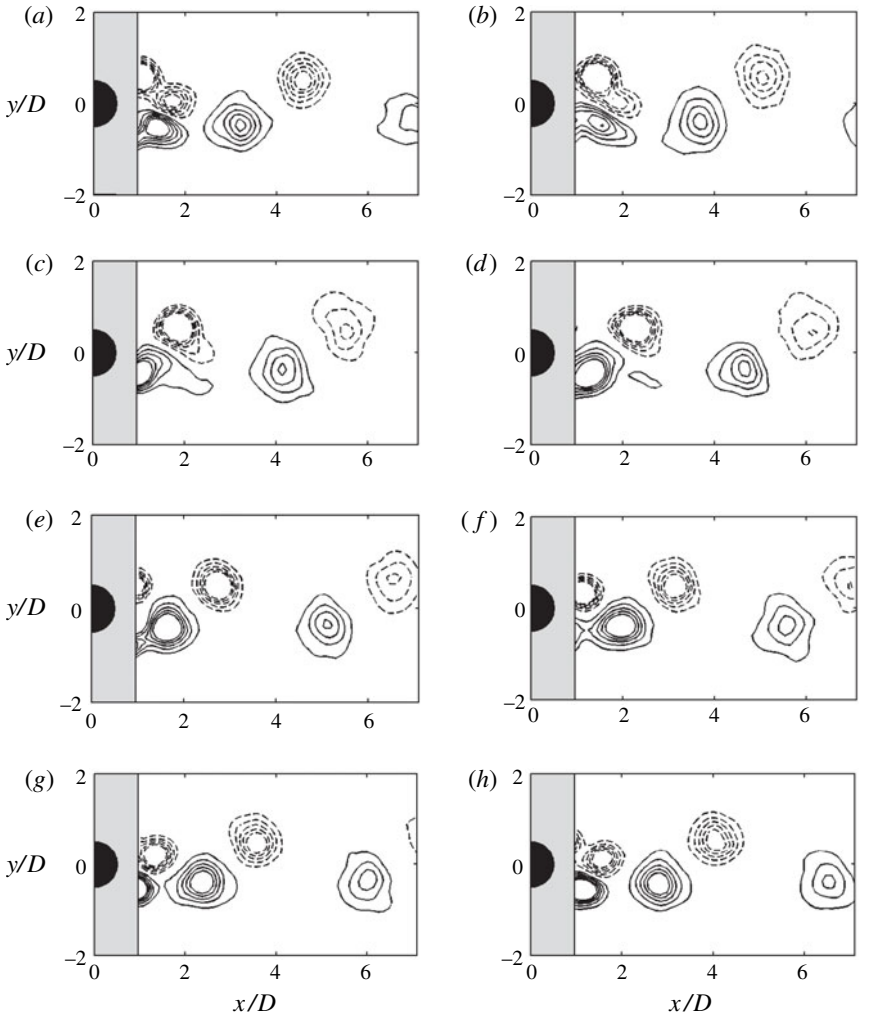


FIGURE 11. Phase-averaged Ω for a heated cylinder: (*a*) $\Phi = 0$; (*b*) $\Phi = \pi/2$; (*c*) $\Phi = \pi$; (*d*) $\Phi = 3\pi/2$; (*e*) $\Phi = 2\pi$; (*f*) $\Phi = 5\pi/2$; (*g*) $\Phi = 3\pi$; and (*h*) $\Phi = 7\pi/2$. Cylinder forced at $\theta_{PP} = 1.05$, $F_R = 2.12$. Phase averaged over two oscillation cycles.

seen even far downstream from the cylinder. This is expected since the vorticity fields show strong, coherent vortical structures that are locked-on to the cylinder forcing even at streamwise locations more than eight cylinder diameters downstream.

In the subharmonic range ($F_R < 1.0$) there is a sharp transition from the lock-on regime to the non-lock-on regime. This is seen in both cases, heated and unheated cylinder. While these kind of sharp transitions have been observed at lower *Re* for an unheated cylinder (Sellappan & Pottebaum 2014) and it is not surprising to observe it for an unheated cylinder at $Re = 750$, in the present study, it was also observed for a heated cylinder. Previous studies that looked at transversely oscillating cylinders found that in the case of a heated cylinder the transition regions are mostly smooth, with some test cases on the boundary even exhibiting a periodic mode switching (Pottebaum 2003). It is possible that a narrow transition region does exist for a

https://doi.org/10.1017/jfm.2014.191 Published online by Cambridge University Press

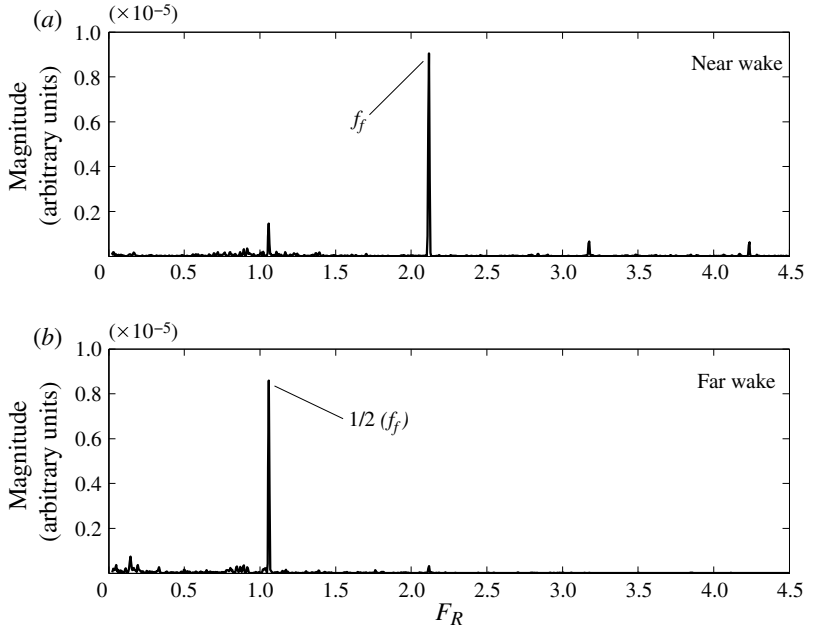


FIGURE 12. Spectra measured along $y/D = 0.45$ at streamwise locations (*a*) $x/D = 1.08$ and (*b*) $x/D = 4.60$. Cylinder is heated. Cylinder forced at $\theta_{PP} = 1.05$, $F_R = 2.12$.

heated cylinder, but the test case density in the parameter space is insufficient to detect it. If that is the case, the relative narrowness of the transition region also implies a fundamental difference in the stability characteristics of the wake of a rotationally oscillating cylinder compared with that of the wake of a transversely oscillating cylinder. A detailed stability analysis is required to provide a definitive explanation.

Region (*b*), labelled as a 'non-lock-on region' in the wake mode maps given in figure 4, extends on both sides of the lock-on region and has a non-locked-on wake mode. In the subharmonic range, it extends to higher amplitudes as F_R decreases. For $F_R > 1.0$, for both the unheated and heated cylinder, the non-lock-on regions exhibit similar trends, with some minor differences. In both cases, the maximum amplitude up to which it extends is approximately around $\theta_{PP} = 0.75$. Near the harmonics the extent of the non-lock-on region is much lower. This is different from the wake mode boundaries observed at $Re = 150$, where, below a certain threshold amplitude value, the flow is always non-locked-on except for a small region around the second harmonic (Sellappan & Pottebaum 2014). At $Re = 750$, there are locked-on wake modes near both the first and second harmonic. Figure 7 shows the phase-averaged vorticity fields seen in the wake of an unheated cylinder for the non-locked-on case, $\theta_{PP} = 0.17$ and $F_R = 1.87$, and figure 8 shows the power spectra for the same case. The vorticity fields are phase-averaged over one cylinder oscillation cycle. The phase-averaged vorticity plots show no coherent, locked-on structures in the wake and, since the individual vortices shed are not in-phase with the forcing, phase-averaging leads to contour plots that contain elongated, 'smeared out' structures that seem to originate from either side of the cylinder. These structures do not exhibit the vortex roll-up and shedding sequence seen in the case of locked-on wakes, and are essentially

https://doi.org/10.1017/jfm.2014.191 Published online by Cambridge University Press

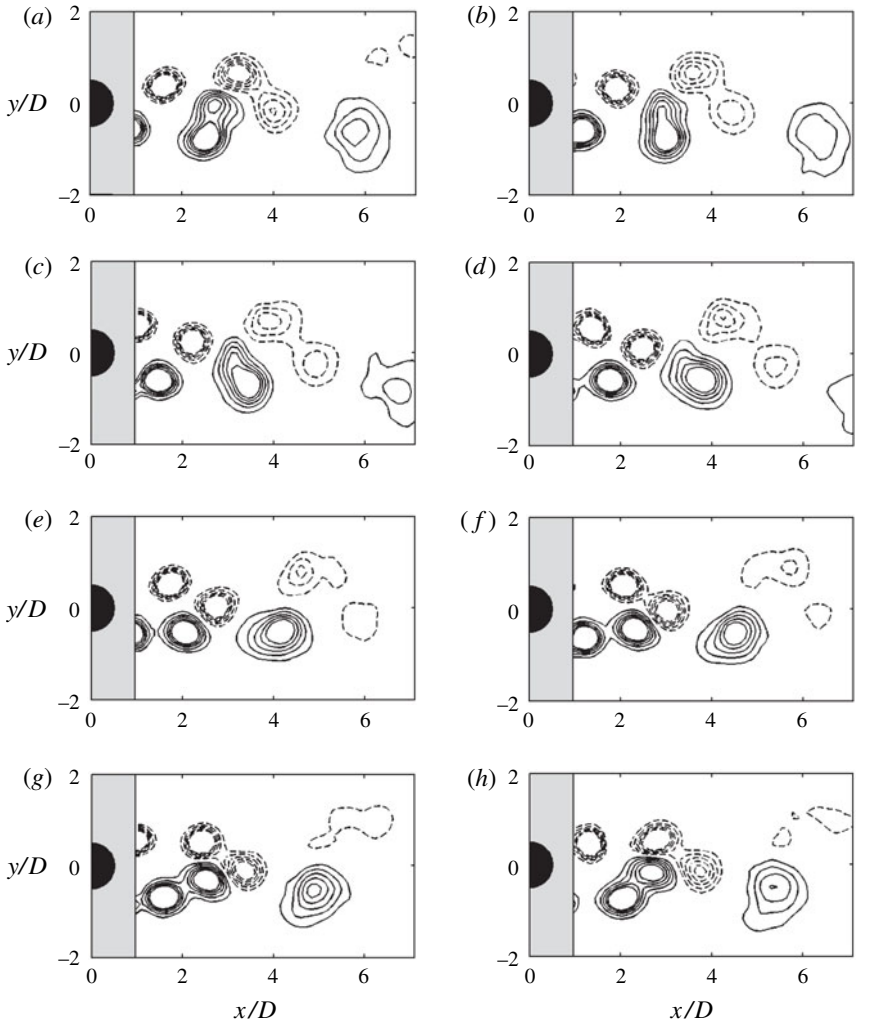


FIGURE 13. Phase-averaged Ω for an unheated cylinder: (*a*) $\Phi = 0$; (*b*) $\Phi = \pi/2$; (*c*) $\Phi = \pi$; (*d*) $\Phi = 3\pi/2$; (*e*) $\Phi = 2\pi$; (*f*) $\Phi = 5\pi/2$; (*g*) $\Phi = 3\pi$; and (*h*) $\Phi = 7\pi/2$. Cylinder forced at $\theta_{PP} = 1.40$, $F_R = 2.12$. Phase averaged over two oscillation cycles.

an artifact of the averaging. Close to the cylinder, the dominant peak in the power spectra is at the Strouhal frequency, f_S, for both the heated and unheated cylinders. At locations further downstream, the power spectrum has complex frequency content consisting of f_S, harmonics and other unrelated frequencies.

3.1.2. *Wake modes at higher forcing frequencies: 'Near-wake* 2S*, far-wake non-locked-on'*

At higher forcing frequencies ($F_R > 1.5$), most cases belong to region (*c*) in the wake mode maps given in figure 4. Phase averaging of cases in this region reveals that over one oscillation cycle two single vortices (2S) are shed and the vortices coalesce to form a far-wake that is not locked-on to the cylinder forcing. Figure 9 shows the phase-averaged vorticity fields seen in the wake of a heated cylinder for cylinder

https://doi.org/10.1017/jfm.2014.191 Published online by Cambridge University Press

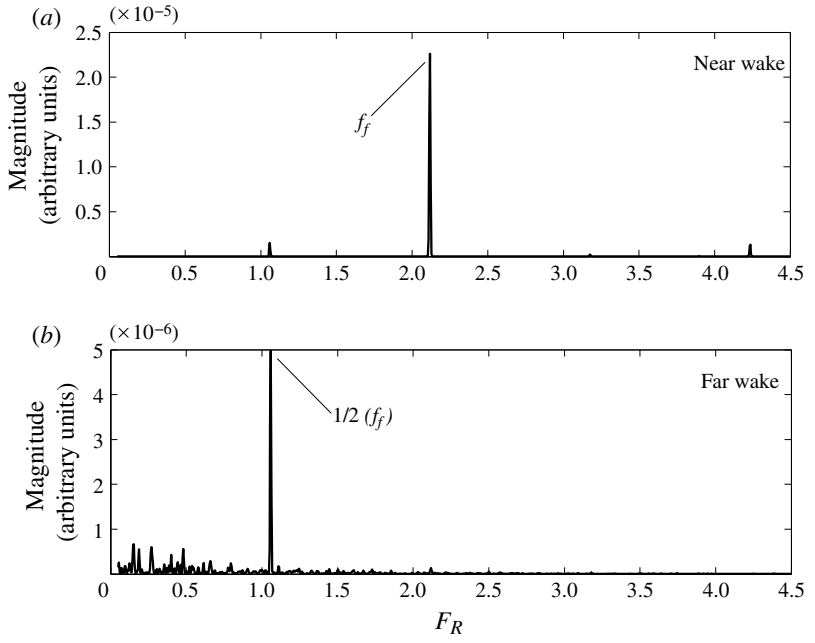


FIGURE 14. Spectra measured along $y/D = -1.08$ at streamwise locations (*a*) $x/D = 1.32$ and (*b*) $x/D = 4.83$. Cylinder is unheated. Cylinder forced at $\theta_{PP} = 1.40$, $F_R = 2.12$.

forcing conditions $\theta_{PP} = 1.40$ and $F_R = 2.72$, and figure 10 shows the power spectra for the same case. In the near-wake, a 2S wake mode is present, but between $2D$ and $4D$ the vortices coalesce together. The vortex structures further downstream are not locked-on to the cylinder forcing and, as a result of phase averaging, appear smeared out in the far-wake. The power spectra confirm the dominant frequency in the near-wake to be the forcing frequency, which implies that the vortex shedding is locked-on to the cylinder forcing. Downstream of the coalescence location, in the far-wake, the power spectra are more complex with dominant peaks at multiple frequencies which indicate that the wake is not locked-on to the cylinder forcing.

3.1.3. *Wake modes near the first harmonic:* (1/2)(2S) *far-wake mode*

Region (*d*) in the wake mode maps given in figure 4 denotes cases in which the near-wake has a 2S wake mode, which is unstable and coalesces to form a far-wake that has a 2S wake mode over two oscillation cycles. This can be readily seen in the phase-averaged vorticity plots, with phase averaging performed over two cycles. Figure 11 shows the phase-averaged vorticity fields of a heated cylinder for the forcing conditions, $\theta_{PP} = 1.05$ and $F_R = 2.12$, and figure 12 shows the power spectra for the same test case. The spectral data show that the dominant frequency in the near-wake is the forcing frequency. This agrees with the phase-averaged vorticity plots which show four single vortices, two of each sense, shed over two cycles. In the far-wake, the spectral data contain a dominant peak at a frequency that is half of the forcing frequency and this is consistent with the phase-averaged vorticity plots which show a 2S mode locked-on over two cycles.

https://doi.org/10.1017/jfm.2014.191 Published online by Cambridge University Press

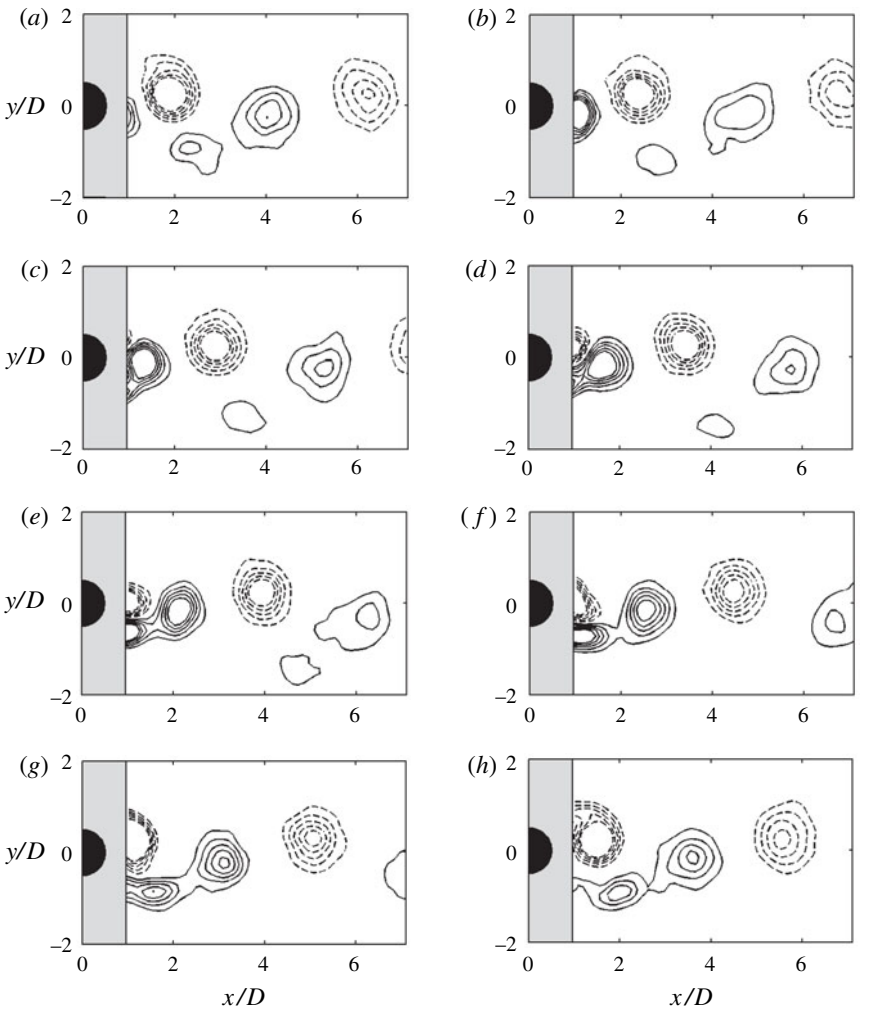


FIGURE 15. Phase-averaged Ω for a heated cylinder: (*a*) $\Phi = 0$; (*b*) $\Phi = \pi/2$; (*c*) $\Phi = \pi$; (*d*) $\Phi = 3\pi/2$; (*e*) $\Phi = 2\pi$; (*f*) $\Phi = 5\pi/2$; (*g*) $\Phi = 3\pi$; and (*h*) $\Phi = 7\pi/2$. Cylinder forced at $\theta_{PP} = 0.87$, $F_R = 1.87$. Phase averaged over two oscillation cycles.

3.1.4. *Wake modes near first harmonic:* (1/2)(P + S) *far-wake mode*

This region, region (*e*), is labelled as '(1/2)(P + S) far-wake mode' in the wake mode maps given in figure 4. The near-wake in this region has a 2S wake mode, which is unstable and coalesces to form a far-wake that has a P + S wake mode that is locked-on over two oscillation cycles. This can be seen only in the phase-averaged vorticity plots, with phase averaging performed over two cycles. Figure 13 shows the phase-averaged vorticity fields of an unheated cylinder for the forcing conditions, $\theta_{PP} = 1.40$ and $F_R = 2.12$, and figure 14 shows the power spectra for the same test case. Similar to the '(1/2)(2S) far-wake mode' region, the power spectra in this region indicate that the forcing frequency is dominant in the near-wake, and this is consistent with the phase-averaged vorticity plots which show that four single vortices, two of each sense, are shed over two cycles. In the far-wake, the spectral data contains a dominant peak at a frequency that is half of the forcing frequency which suggests

https://doi.org/10.1017/jfm.2014.191 Published online by Cambridge University Press

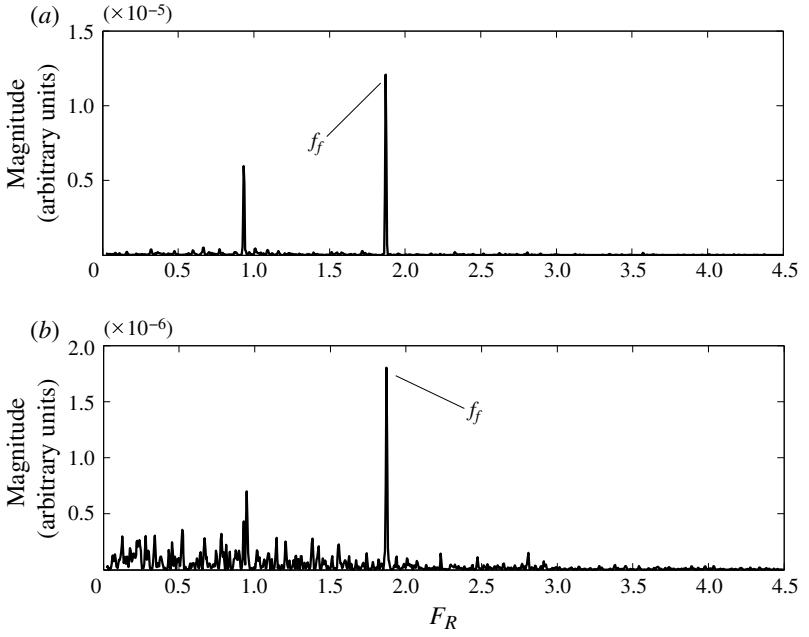


FIGURE 16. Spectra measured along $y/D = -0.37$ at streamwise locations (*a*) $x/D = 1.32$ and (*b*) $x/D = 3.66$. Cylinder is heated. Cylinder forced at $\theta_{PP} = 0.87$, $F_R = 1.87$.

that the far-wake is again 2S over two cycles. However, the phase-averaged vorticity plots show that only counter-clockwise rotating vortices coalesce together to form a single vortex while the clockwise rotating vortices, whose contours are indicated by dashed lines, do not merge together completely. Instead, as they start to coalesce, the leading vortex is pulled away by the single vortex of the opposite sense formed by coalescence during the previous cycle, to form a pair (P) of counter-rotating vortices. It was also observed that for a disproportionate number of cases in this region, the single vortex (S) in the P + S mode was formed by the clockwise rotating vortex, as described above, and this trend was reversed, when the cylinder oscillations were started in the opposite direction. This implies that wake formation is extremely sensitive to initial conditions.

3.1.5. *Wake modes near the first harmonic:* (1/2)(P + S) *wake mode, no coalescence*

Region (*f*) in the wake mode maps given in figure 4 is a locked-on wake mode region present around the first harmonic, and it denotes a region in which no coalescence of vortices was observed. Phase-averaging vorticity fields over a single cycle shows a non-locked-on wake, but phase averaging performed over two cycles reveals a P + S locked-on wake mode. Figure 15 shows the vorticity fields phase-averaged over two cycles for a heated cylinder under the forcing conditions, $\theta_{PP} = 0.87$ and $F_R = 1.87$, and figure 16 shows the power spectra for the same test case. The power spectra contain dominant peaks at the forcing frequency and at half the forcing frequency, which indicate the occurrence of locked-on structures at twice the oscillation period. Phase-averaged vorticity plots show that over two cycles three vortices are shed. Two vortices are of the same rotational sense and the other is of the opposite sense. The leading vortex, among the two single vortices of the

https://doi.org/10.1017/jfm.2014.191 Published online by Cambridge University Press

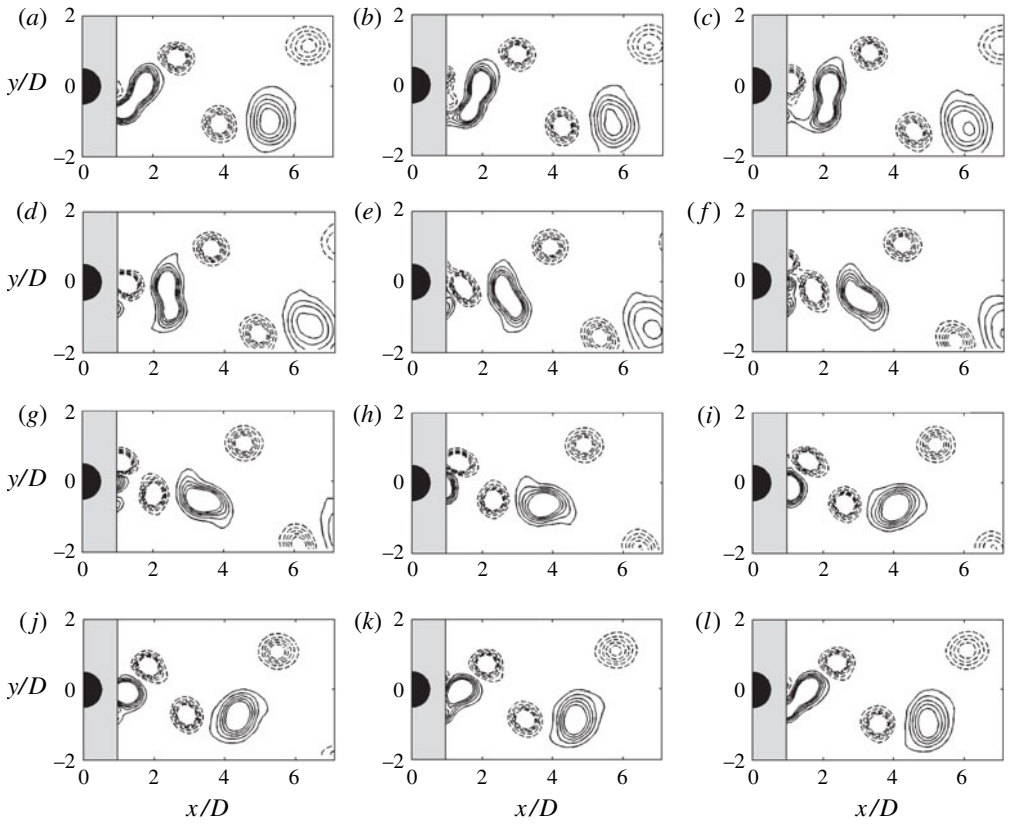


FIGURE 17. Phase-averaged Ω for an unheated cylinder: (*a*) $\Phi = 0$; (*b*) $\Phi = \pi/2$; (*c*) $\Phi = \pi$; (*d*) $\Phi = 3\pi/2$; (*e*) $\Phi = 2\pi$; (*f*) $\Phi = 5\pi/2$; (*g*) $\Phi = 3\pi$; (*h*) $\Phi = 7\pi/2$; (*i*) $\Phi = 4\pi$; (*j*) $\Phi = 9\pi/2$; (*k*) $\Phi = 5\pi$; and (*l*) $\Phi = 11\pi/2$. Cylinder forced at $\theta_{PP} = 0.52$, $F_R = 3.16$. Phase averaged over three oscillation cycles.

same sense, is pulled away by the third vortex to form a pair. Again, the unheated and heated cylinder wakes are similar, with asymmetric shedding in one direction preferred over the other, and the initial oscillation direction affects this asymmetry.

3.1.6. *Wake modes near the second harmonic:* (1/3)(P + S) *wake mode, no coalescence*

Region (*g*), '(1/3)(P + S), no coalescence', in the wake mode maps given in figure 4 is present near the second harmonic and is a locked-on mode. No coalescence was observed in this region. Phase-averaging over three oscillation cycles shows a P + S wake mode that is locked-on to the cylinder forcing. Figure 17 shows the vorticity fields phase-averaged over three cycles for an unheated cylinder under the forcing conditions, $\theta_{PP} = 0.52$ and $F_R = 3.16$. Figure 18 shows the power spectra for the same test case. When phase-averaged over one or two cycles, the wake structure looks similar to a non-locked-on wake, but when phase-averaged over three cycles, the vorticity fields show that three vortices are shed over three oscillation cycles. The spectral data show peaks at f_f, $(1/2)f_f$ and $(1/3)f_f$, with the peak at $(1/3)f_f$ being the most dominant. This indicates the occurrence of wake structures synchronized over three times the oscillation period. As observed in other regions, the wake of the heated cylinder was found to be very similar to the wake of the unheated cylinder.

https://doi.org/10.1017/jfm.2014.191 Published online by Cambridge University Press

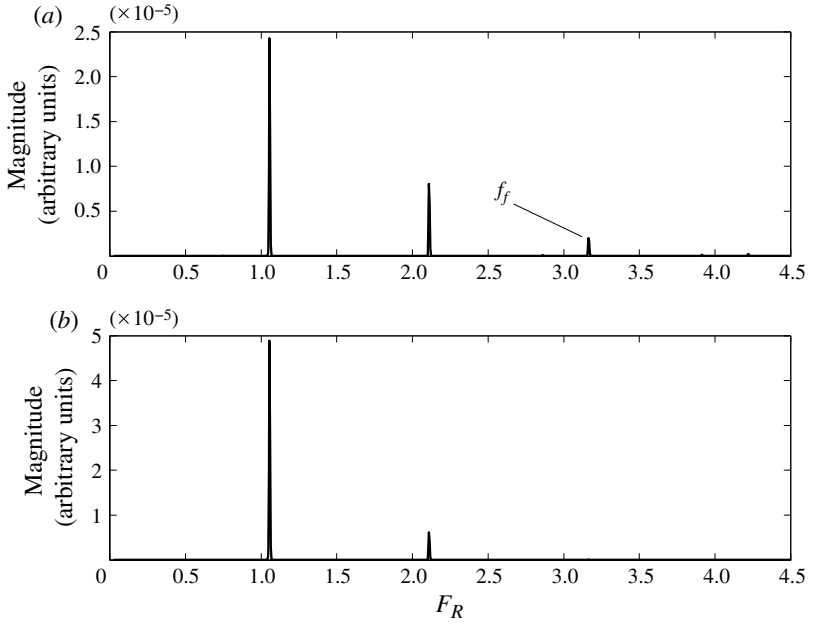


FIGURE 18. Spectra measured along $y/D = -0.02$ at streamwise locations (*a*) $x/D = 1.55$ and (*b*) $x/D = 3.89$. Cylinder is unheated. Cylinder forced at $\theta_{PP} = 0.52$, $F_R = 3.16$.

3.1.7. *Wake modes near the second harmonic:* (1/3)(2P) *wake mode, no coalescence*

Another locked-on wake mode region near the second harmonic is region (*h*), labelled '(1/3)(2P), no coalescence', in the wake mode maps given in figure 4. No coalescence was observed in this region and phase-averaging vorticity fields over one and two oscillation cycles shows a non-locked-on wake. Phase-averaging over three oscillation cycles shows a 2P wake mode that is synchronized with the cylinder forcing. Figure 19 shows the vorticity fields phase-averaged over three cycles for an unheated cylinder under the forcing conditions, $\theta_{PP} = 0.70$ and $F_R = 3.06$. The power spectra for the same case is shown in figure 20. The phase-averaged vorticity plots clearly show that four vortices are shed over three cycles and each vortex pairs up with a vortex of the opposite sense to form a pair. Therefore, two pairs are formed over three cycles. This is true for both the unheated cylinder wake and the heated cylinder wake and the spectral data for both show peaks at f_f, $(1/2)f_f$ and $(1/3)f_f$. The dominant peaks in both cases are at a third of the forcing frequency and at half the forcing frequency. This is indicative of a 2P mode synchronized over three cycles. This region is relatively small and occurs at very low oscillation amplitude in the parameter space and, especially for the unheated cylinder, it is extremely narrow. In both cases, it is centred on the second harmonic and the presence of the harmonic is conjectured to play a role in the occurrence of this stable, locked-on wake mode.

3.2. *Heat transfer from cylinder and its dependence on forcing conditions*

Figure 21 shows a contour plot of normalized heat transfer (Nu/Nu_0) with the wake mode boundaries of a heated cylinder given in figure 4(*b*) superimposed on it. The heat-transfer rate (Nu) is normalized using the heat-transfer rate of the stationary

https://doi.org/10.1017/jfm.2014.191 Published online by Cambridge University Press

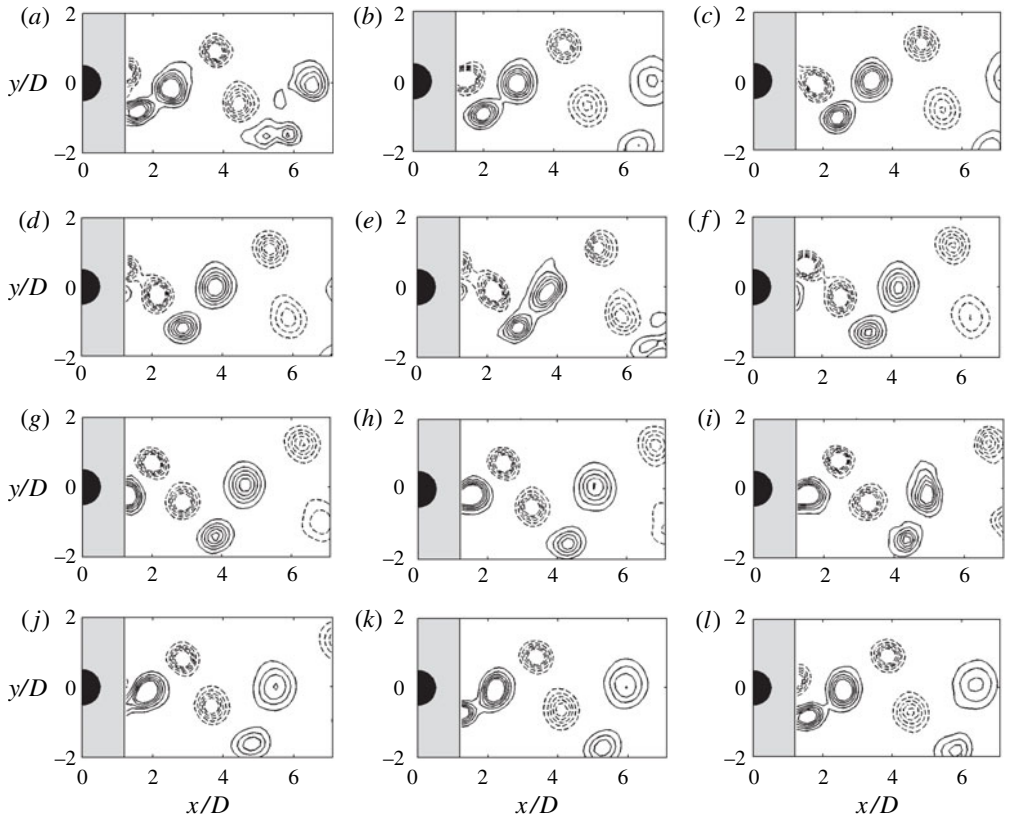


FIGURE 19. Phase-averaged Ω for an unheated cylinder: (*a*) $\Phi = 0$; (*b*) $\Phi = \pi/2$; (*c*) $\Phi = \pi$; (*d*) $\Phi = 3\pi/2$; (*e*) $\Phi = 2\pi$; (*f*) $\Phi = 5\pi/2$; (*g*) $\Phi = 3\pi$; (*h*) $\Phi = 7\pi/2$; (*i*) $\Phi = 4\pi$; (*j*) $\Phi = 9\pi/2$; (*k*) $\Phi = 5\pi$; and (*l*) $\Phi = 11\pi/2$. Cylinder forced at $\theta_{PP} = 0.70$, $F_R = 3.06$. Phase averaged over three oscillation cycles.

cylinder ($Nu_0 \approx 24.3$). The occurrence of heat-transfer enhancement, or the lack thereof, in certain regions of the parameter space suggests that cylinder forcing may be affecting it. It was shown in the previous subsections that wake formation also depends on the cylinder forcing conditions. So it is possible that wake formation and heat transfer are closely related. The most prominent features that are noticeable in figure 21 are the regions with high heat transfer. All of these regions are located at or near the Strouhal frequency and its harmonics and this suggests some form of synchronization between the heat transfer and the harmonics. It is also apparent that certain wake modes correlate to regions with significant heat-transfer enhancement. The most significant region of heat-transfer enhancement is around the Strouhal frequency, which is expected since the vortex shedding seen in this region is highly synchronized with the cylinder forcing leading to the formation of a locked-on 2S wake mode. There is also significant heat-transfer enhancement around the first and second harmonic and this correlates with locked-on wake modes. Near the second harmonic, the (1/3)(P + S) and (1/3)(2P) wake modes are of particular interest since they occur at very low oscillation amplitudes and, as a result, would not normally be expected to have a high heat-transfer rate. It is speculated that the occurrence of locked-on wake modes is the reason for the heat-transfer enhancement that is

https://doi.org/10.1017/jfm.2014.191 Published online by Cambridge University Press

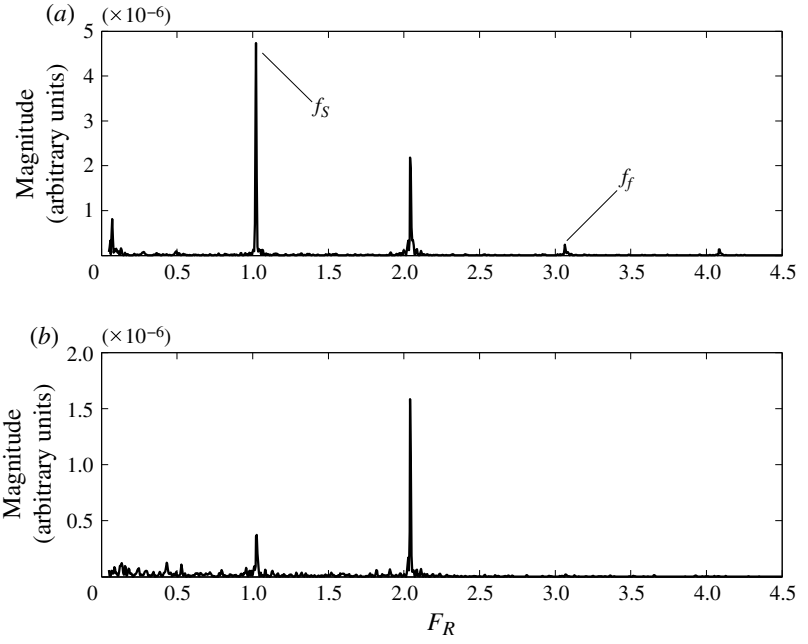


FIGURE 20. Spectra measured along $y/D = -0.31$ at streamwise locations (*a*) $x/D = 1.86$ and (*b*) $x/D = 5.35$. Cylinder is unheated. Cylinder forced at $\theta_{PP} = 0.70$, $F_R = 3.06$.

observed. The locked-on wake modes are generally effective at removing fluid away from the cylinder base, leading to relatively cooler fluid coming in contact with the cylinder, and this in turn leads to a higher than normal temperature difference between the surface of the cylinder and the surrounding fluid and the resultant increase in heat-transfer rate.

Around the first harmonic the correlation between wake modes and heat-transfer enhancement is not straightforward. While the '(1/2)(P + S), no coalescence' wake mode region displays heat-transfer enhancement, the '(1/2)(2S) far-wake mode' region does so to a lesser extent and the '(1/2)(P + S) far-wake mode' region displays an unexpectedly low level of heat-transfer enhancement above the norm considering its high oscillation amplitude. The 2S mode near the Strouhal frequency is efficient at removing fluid from near the cylinder and this increases the heat-transfer rate. The '(1/2)(2S) far-wake mode' region and the '(1/2)(P + S) far-wake mode' region both possess a locked-on 2S mode in the near-wake. While the near-wake exhibits what looks like a 2S mode, it is unstable and not completely locked-on and this could lead to the lower than expected heat-transfer enhancement. It is also possible that the vortex roll-up distance is generally longer around the first harmonic, leading to less effective removal of fluid from the 'dead-water' region and a correspondingly lower heat-transfer enhancement.

The low level of heat-transfer enhancement, barely higher than that of a stationary cylinder, seen in the non-locked-on region (*b*) is not surprising given the low amplitudes and/or low frequencies of oscillation for cases in this region. Conversely, the enhanced heat-transfer rates seen in certain parts of region (*c*) can be attributed to the relatively high forcing frequency and amplitude. However, there are also parts of region (*c*) which exhibit low levels of heat transfer despite relatively high forcing

https://doi.org/10.1017/jfm.2014.191 Published online by Cambridge University Press

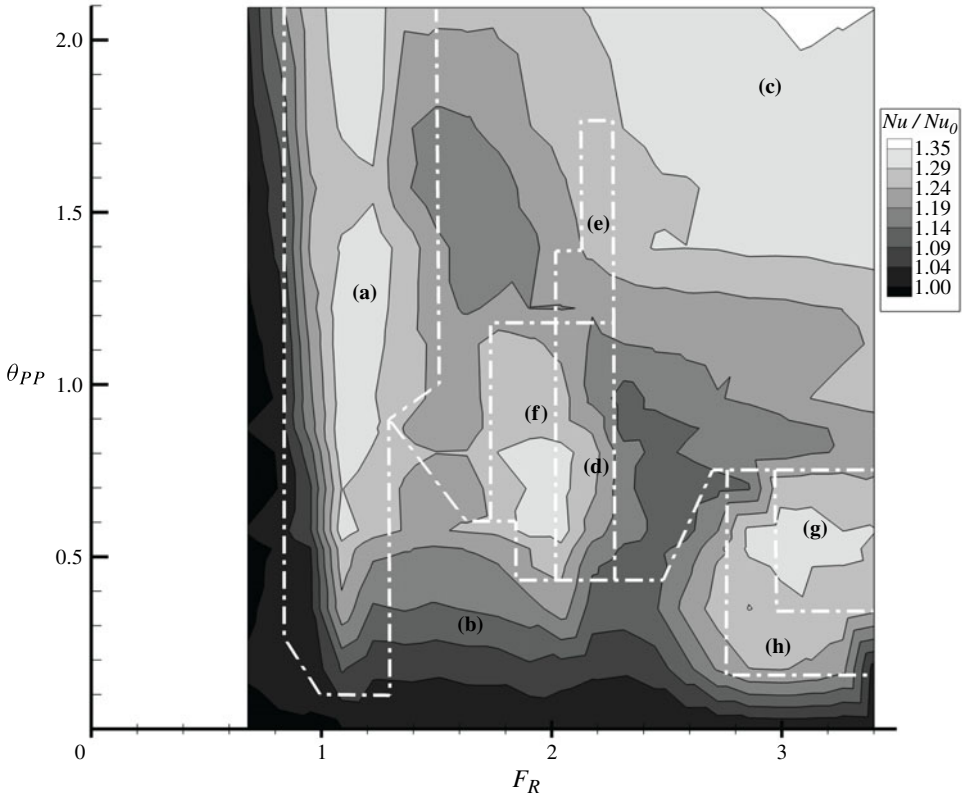


FIGURE 21. Contours of normalized heat transfer (Nu/Nu_0) with wake mode boundaries superimposed. Contour levels are spaced exponentially with the lowest contour level being unity. Dashed and dotted white lines are wake mode boundaries. Wake mode regions labelled as in figure 4.

frequency or amplitude. It implies the existence of another parameter that would account for these results. Pottebaum (2003) found that in the case of transversely oscillating cylinders, the transverse velocity is related to heat-transfer enhancement in certain regions of the parameter space. It is possible that a similar relationship exists in the case of rotationally oscillating cylinders too. Since the cylinder motion is sinusoidal, the root-mean-square (r.m.s.) tangential velocity (V_{rms}) on the surface of the cylinder is equal to $1/\sqrt{2}$ times the peak tangential velocity on the surface of the cylinder, and $V_{rms}/U_0 = (f_S \pi D/2\sqrt{2}U_0)(F_R)(\theta_{PP}) = 0.220(F_R)(\theta_{PP})$. The normalized heat-transfer rate (Nu/Nu_0) is plotted as a function of the normalized r.m.s. tangential velocity (V_{rms}/U_0) in figure 22. The wake mode of each case is also identified. The locked-on modes exhibit significant heat-transfer enhancement as expected and also exhibit significant scatter when $V_{rms}/U_0 < 1$. But for $V_{rms}/U_0 > 1$, the data partially collapses. Almost all of the cases from region (*c*) follow this collapsed path. Away from locked-on wake mode regions, and especially for cases in region (*c*), the tangential velocity on the cylinder surface is an important factor that determines the heat-transfer rate. Note that all of the cases from region (*e*), '(1/2)(P + S) far-wake mode', also collapse onto this path, so heat transfer is determined predominantly by the tangential velocity, in spite of the wake mode synchronization.

https://doi.org/10.1017/jfm.2014.191 Published online by Cambridge University Press

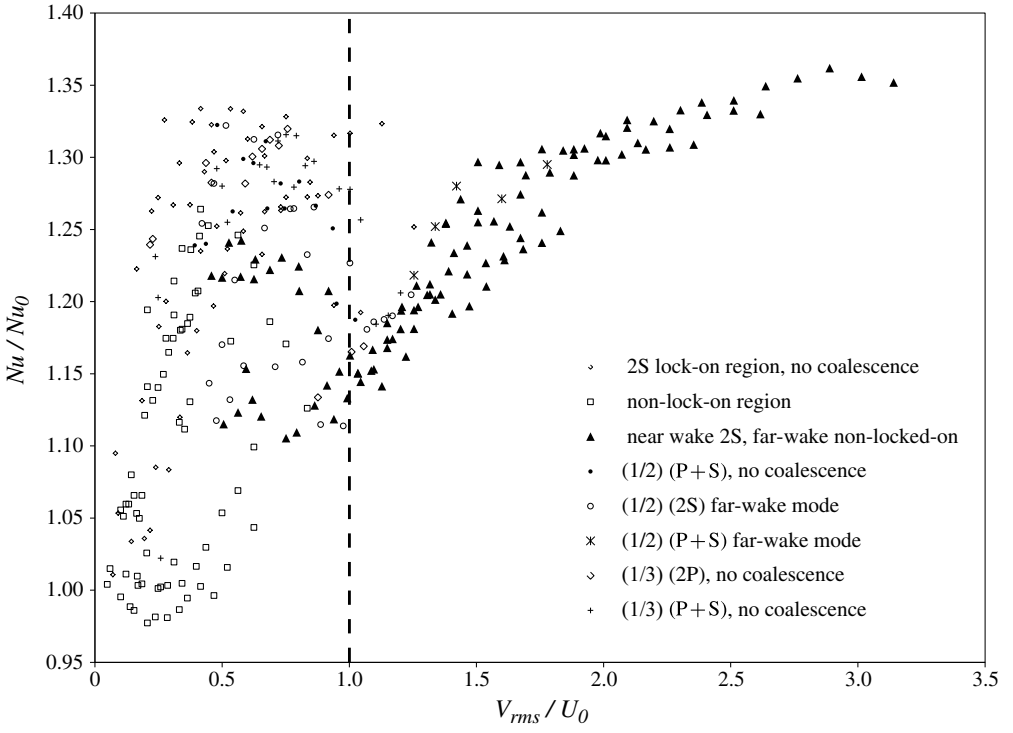


FIGURE 22. Normalized heat-transfer rate (Nu/Nu_0) versus normalized r.m.s. tangential velocity (V_{rms}/U_0), with individual wake modes identified.

4. Conclusions

The effects of rotary forcing on vortex shedding and heat transfer from the cylinder were studied. The effect of rotary forcing on heat-transfer rate was found to be quite profound at certain forcing conditions. Significant heat-transfer enhancement was observed when the forcing frequency was comparable to the Strouhal frequency. Significant regions of heat-transfer enhancement were also discovered around the first and second harmonics. The forcing amplitude was also found to play a role in determining the heat-transfer rates, with heat-transfer enhancement occurring only above a certain amplitude even when $f_f \approx f_S$.

Experiments were also performed to study vortex shedding from unheated and heated cylinders and the flow field information obtained through DPIV lead to the discovery of wake modes synchronized over single and multiple oscillation cycles. At higher forcing frequencies coalescence was observed, leading to locked-on far-wake structures in certain cases. Locked-on wakes, which did not exhibit coalescence, were also observed around the second harmonic. Certain locked-on wake modes also correlate to regions of heat-transfer enhancement. It was found that inclusion of heat transfer in the wake formation process did not lead to any new wake modes. It did lead to changes in the size, shape and specific location of wake mode boundaries in the parameter space for a heated cylinder when compared to an unheated cylinder, but the general location of these wake mode regions with respect to the Strouhal frequency and its harmonics remained more or less constant. The mode-switching phenomenon observed in previous studies with heated, transversely oscillating cylinders was not

https://doi.org/10.1017/jfm.2014.191 Published online by Cambridge University Press

observed in the present study. Instead, sharp transitions were observed between wake mode regions.

At higher rotation rates the heat transfer is strongly affected by the local surface shear magnitude. In particular, for cases that exhibit a non-locked-on far-wake, when $V_{rms}/U_0 > 1.0$, the cylinder surface tangential velocity was found to play an important role in determining the heat-transfer rate. At the other end of the scale, even for low values of V_{rms}/U_0, wake mode synchronization leads to significant heat-transfer enhancement.

Acknowledgements

The first author would like to thank Professor Geoff Spedding for his assistance with the DPIV technique and for his helpful comments concerning the manuscript. The authors would also like to thank the referees for their helpful comments and suggestions.

REFERENCES

BAEK, S. J. & SUNG, H. J. 2000 Quasi-periodicity in the wake of a rotationally oscillating cylinder. *J. Fluid Mech.* **408**, 275–300.

BEARMAN, P. W. 1969 On vortex shedding from a circular cylinder in critical Reynolds number regime. *J. Fluid Mech.* **37** (3), 577–585.

BOUHAIRIE, S. & CHU, V. H. 2007 Two-dimensional simulation of unsteady heat transfer from a circular cylinder in crossflow. *J. Fluid Mech.* **570**, 177–215.

CHANG, B. H. & MILLS, A. F. 2004 Effect of aspect ratio on forced convection heat transfer from cylinders. *Intl J. Heat Mass Transfer* **47** (6–7), 1289–1296.

DENNIS, S. C. R., NGUYEN, P. & KOCABIYIK, S. 2000 The flow induced by a rotationally oscillating and translating circular cylinder. *J. Fluid Mech.* **407**, 123–144.

DU, L. & DALTON, C. 2013 LES calculation for uniform flow past a rotationally oscillating cylinder. *J. Fluids Struct.* **42**, 40–54.

EISENLOHR, H. & ECKELMANN, H. 1989 Vortex splitting and its consequences in the vortex street wake of cylinders at low Reynolds number. *Phys. Fluids* A **1** (2), 189–192.

FUJISAWA, N., KAWAJI, Y. & IKEMOTO, K. 2001 Feedback control of vortex shedding from a circular cylinder by rotational oscillations. *J. Fluids Struct.* **15** (1), 23–37.

FUJISAWA, N., TANAHASHI, S. & SRINIVAS, K. 2005 Evaluation of pressure field and fluid forces on a circular cylinder with and without rotational oscillation using velocity data from PIV measurement. *Meas. Sci. Technol.* **16** (4), 989–996.

HAMMACHE, M. & GHARIB, M. 1989 A novel method to promote parallel vortex shedding in the wake of circular cylinders. *Phys. Fluids* A **1** (10), 1611–1614.

HE, J. W., GLOWINSKI, R., METCALFE, R., NORDLANDER, A. & PERIAUX, J. 2000 Active control and drag optimization for flow past a circular cylinder I. Oscillatory cylinder rotation. *J. Comput. Phys.* **163** (1), 83–117.

HU, H. & KOOCHESFAHANI, M. M. 2011 Thermal effects on the wake of a heated circular cylinder operating in mixed convection regime. *J. Fluid Mech.* **685**, 235–270.

INCROPERA, F. P. & DEWITT, D. P. 1996 *Fundamentals of Heat and Mass Transfer*. 4th edn John Wiley & Sons, New York.

JIAN, D., XUE-MING, S. & AN-LU, R. 2007 Vanishing of three-dimensionality in the wake behind a rotationally oscillating circular cylinder. *J. Hydrodyn.* B **19** (6), 751–755.

KUMAR, S., LOPEZ, C., PROBST, O., FRANCISCO, G., ASKARI, D. & YANG, Y. 2013 Flow past a rotationally oscillating cylinder. *J. Fluid Mech.* **735**, 307–346.

KWON, K. & CHOI, H. 1996 Control of laminar vortex shedding behind a circular cylinder using splitter plates. *Phys. Fluids* **8** (2), 479–486.

LEE, S. J. & LEE, J. Y. 2006 Flow structure of wake behind a rotationally oscillating circular cylinder. *J. Fluids Struct.* **22** (8), 1097–1112.

https://doi.org/10.1017/jfm.2014.191 Published online by Cambridge University Press

LEE, S. J. & LEE, J. Y. 2008 PIV measurements of the wake behind a rotationally oscillating circular cylinder. *J. Fluids Struct.* **24** (1), 2–17.

LO JACONO, D., LEONTINI, J. S., THOMPSON, M. C. & SHERIDAN, J. 2010 Modification of three-dimensional transition in the wake of a rotationally oscillating cylinder. *J. Fluid Mech.* **643**, 349–362.

LU, L., QIN, J.-M., TENG, B. & LI, Y.-C. 2011 Numerical investigations of lift suppression by feedback rotary oscillation of circular cylinder at low Reynolds number. *Phys. Fluids* **23** (3), 033601.

LU, X. Y. & SATO, J. 1996 A numerical study of flow past a rotationally oscillating circular cylinder. *J. Fluids Struct.* **10** (8), 829–849.

MAHFOUZ, F. M. & BADR, H. M. 2000*a* Flow structure in the wake of a rotationally oscillating cylinder. *Trans. ASME J. Fluids Engng* **122** (2), 290–301.

MAHFOUZ, F. M. & BADR, H. M. 2000*b* Forced convection from a rotationally oscillating cylinder placed in a uniform stream. *Intl J. Heat Mass Transfer* **43** (17), 3093–3104.

MORGAN, V. T. 1975 The overall convective heat transfer from smooth circular cylinders. *Adv. Heat Transfer* **11**, 199–264.

NAZARINIA, M., LO JACONO, D., THOMPSON, M. C. & SHERIDAN, J. 2012 Flow over a cylinder subjected to combined translational and rotational oscillations. *J. Fluids Struct.* **32**, 135–145.

NISHIHARA, T., KANEKO, S. & WATANABE, T. 2005 Characteristics of fluid dynamic forces acting on a circular cylinder oscillated in the streamwise direction and its wake patterns. *J. Fluids Struct.* **20** (4), 505–518.

NORBERG, C. 1994 An experimental investigation of the flow around a circular-cylinder—influence of aspect ratio. *J. Fluid Mech.* **258**, 287–316.

NORBERG, C. 2001 Flow around a circular cylinder: aspects of fluctuating lift. *J. Fluids Struct.* **15**, 459–469.

PONCET, P. 2002 Vanishing of mode B in the wake behind a rotationally oscillating circular cylinder. *Phys. Fluids* **14** (6), 2021–2023.

POSDZIECH, O. & GRUNDMANN, R. 2007 A systematic approach to the numerical calculation of fundamental quantities of the two-dimensional flow over a circular cylinder. *J. Fluids Struct.* **23**, 479–499.

POTTEBAUM, T. 2003 The relationship between near-wake structure and heat transfer for an oscillating circular cylinder in cross-flow. PhD thesis, California Institute of Technology, Pasadena, CA, USA.

POTTEBAUM, T. S. & GHARIB, M. 2006 Using oscillations to enhance heat transfer for a circular cylinder. *Intl J. Heat Mass Transfer* **49** (17–18), 3190–3210.

ROSHKO, A. 1954 *On the Drag and Shedding Frequency of Two-Dimensional Bluff Bodies. Tech. Note.* vol. 3169, Nat. Adv. Comm. Aero.

ROSHKO, A. 1955 On the wake and drag of bluff bodies. *J. Aero. Sci.* **22** (2), 124–132.

ROSHKO, A. 1961 Experiments on the flow past a circular cylinder at very high Reynolds number. *J. Fluid Mech.* **10** (3), 345–356.

SAAD, M., LEE, L. & LEE, T. 2007 Shear layers of a circular cylinder with rotary oscillation. *Exp. Fluids* **43** (4), 569–578.

SELLAPPAN, P. 2013 Wake modes of rotationally oscillating circular cylinder in cross-flow and its relationship with heat transfer. PhD thesis, University of Southern California, Los Angeles, CA, USA.

SELLAPPAN, P. & POTTEBAUM, T. 2014 Wake modes of rotationally oscillating cylinders at $Re = 150$. *J. Fluids Struct.* **46**, 29–41.

SPARROW, E. M., ABRAHAM, J. P. & TONG, J. C. K. 2004 Archival correlations for average heat transfer coefficients for non-circular and circular cylinders and for spheres in cross-flow. *Intl J. Heat Mass Transfer* **47** (24), 5285–5296.

SREENIVASAN, K. & RAMACHANDRAN, A. 1961 Effect of vibration on heat transfer from a horizontal cylinder to a normal air stream. *Intl J. Heat Mass Transfer* **3** (1), 60–67.

SZEPESSY, S. & BEARMAN, P. W. 1992 Aspect ratio and end plate effects on vortex shedding from a circular cylinder. *J. Fluid Mech.* **234**, 191–217.

https://doi.org/10.1017/jfm.2014.191 Published online by Cambridge University Press

THIRIA, B., GOUJON-DURAND, S. & WESFREID, J. E. 2006 The wake of a cylinder performing rotary oscillations. *J. Fluid Mech.* **560**, 123–147.

THIRIA, B. & WESFREID, J. E. 2007 Stability properties of forced wakes. *J. Fluid Mech.* **579**, 137–161.

TOKUMARU, P. T. & DIMOTAKIS, P. E. 1991 Rotary oscillation control of a cylinder wake. *J. Fluid Mech.* **224**, 77–90.

VIT, T., REN, M., TRAVNICEK, Z., MARSIK, F. & RINDT, C. C. M. 2007 The influence of temperature gradient on the Strouhal–Reynolds number relationship for water and air. *Exp. Therm. Fluid Sci.* **31** (7), 751–760.

WILLIAMSON, C. H. K. 1988 Defining a universal and continuous Strouhal–Reynolds number relationship for the laminar vortex shedding of a circular cylinder. *Phys. Fluids* **31** (10), 2742–2744.

WILLIAMSON, C. H. K. 1989 Oblique and parallel modes of vortex shedding in the wake of a circular cylinder at low Reynolds-numbers. *J. Fluid Mech.* **206**, 579–627.

WILLIAMSON, C. H. K. 1996 Vortex dynamics in the cylinder wake. *Annu. Rev. Fluid Mech.* **28**, 477–539.

WILLIAMSON, C. H. K. & ROSHKO, A. 1988 Vortex formation in the wake of an oscillating cylinder. *J. Fluids Struct.* **2** (4), 355–381.

https://doi.org/10.1017/jfm.2014.191 Published online by Cambridge University Press